4-2022

Downscaling of physical risks for climate scenario design

Enrico BIFFIS
Imperial College London

Shuai WANG
Princeton University

Singapore Green Finance Centre

Managed by

Imperial College Business School

SMU Lee Kong Chian School of Business

White Paper

Downscaling of Physical Risks for Climate Scenario Design

4 April 2022

Dr. Enrico BIFFIS
Associate Professor of Actuarial Finance,
Imperial College Business School, Imperial College London

Dr. Shuai WANG
Associate Research Scholar,
Program in Atmospheric and Oceanic Sciences, Princeton University

This work was executed as part of the broader Climate Risk Scenario Workstream designed by Enrico Biffis in collaboration with Raul Rosales at Imperial College London, the MAS and our nine founding partners. We are grateful to **Lim Bey An** and **David Mah** at the Monetary Authority of Singapore, as well as the founding partners who contributed to the October 2021 SGFC workshop on Climate Risk Scenarios, for thoughtful feedback and guidance on design and execution of this deliverable. Any errors remain our own responsibility.

DOWNSCALING OF PHYSICAL RISKS FOR CLIMATE SCENARIO DESIGN

Enrico Biffis[1] and Shuai Wang[2]

Executive summary

Southeast Asia is arguably one of the areas most vulnerable to natural disasters due to its dense population, coastal urbanization, and rainfall variability driven by the local monsoon systems. In this report, we focus on the impact of global warming in the region along four climate dimensions: temperature, precipitation, wind speed and coastal surge. The latter represents the surge of water from the ocean in excess of astronomical tides. Our objective is to downscale the outputs of global climate models to temporal and spatial resolutions of interest to market participants wishing to quantify climate risk vulnerability via climate stress testing exercises truly representative of their exposures *at location*.

Throughout our study, we consider the representative concentration pathway 8.5 until 2050 (referred to as RCP8.5-2050 henceforth), which is widely considered as a high emission scenario and often regarded as capturing the potential failure of the international community to coordinate to implement effective climate risk mitigation policies. As such our focus is broadly consistent with climate scenarios variously referred to as Business As Usual (BAU), No Additional Policy Action (NAPA), or Hot House[3].

Our downscaling approach uses machine learning techniques and places emphasis on the entire distribution of climate variables rather than just the evolution of their average/median level along a climate scenario. We are therefore able to discuss the impact of global warming on both the average level of climate variables of interest and the tail of their distributions. This allows us to disentangle systematic shifts in risk profiles from increases in the frequency and severity of extreme events. We summarize some of the main findings of the report in Figures A to C.

Figure A depicts the changes in the four climate variables of interest across Southeast Asia along RCP8.5-2050. We compare global climate model outputs with those downscaled to a spatial resolution of 1km x 1km, which could be further refined on a demand basis. Results demonstrate how downscaling offers a more granular understanding of physical climate exposures, which can be considerably uneven across geographical areas of interest.

Figure B summarizes the results obtained for Indonesia, Malaysia, Philippines, Thailand. We develop a simple risk rating system indicating the extent to which a country experiences changes in the average vs. tail distribution of four climate variables of interest. Except for the Philippines, all countries experience sizeable increases in average temperature and windspeed. Extreme rainfall events, as opposed to average precipitation, should be the main concern of all countries studied, with Malaysia being the most vulnerable. Coastal surge mainly affects Indonesia and Malaysia, both at the average and tail level.

Figure C offers examples of how downscaling can reveal considerable heterogeneity of exposures at the urban level. We provide tail risk examples for rainfall in Jakarta and Kuala Lumpur, revealing how exposures at location can vary between +100% and -80% relative to the outputs of coarser resolution models. Our study therefore suggests that market participants should rely on properly downscaled average and tail risk parameters to gauge physical risk *at location*.

The final part of the report explores typhoon risk. By projecting and downscaling a key driver of typhoon risk, we find that the region is likely to experience an increase in its frequency and severity.

---

[1] Department of Finance and Brevan Howard Centre for Financial Analysis, Imperial College Business School; Sustainable Tech Lab at I-X, Imperial College London.

[2] Department of Civil and Environmental Engineering, Princeton University.

[3] See, for example, NGFS Climate scenarios for central banks and supervisors (2021) and Bank of England (2021).

Figure A. Downscaling average impact of RCP8.5-2050.

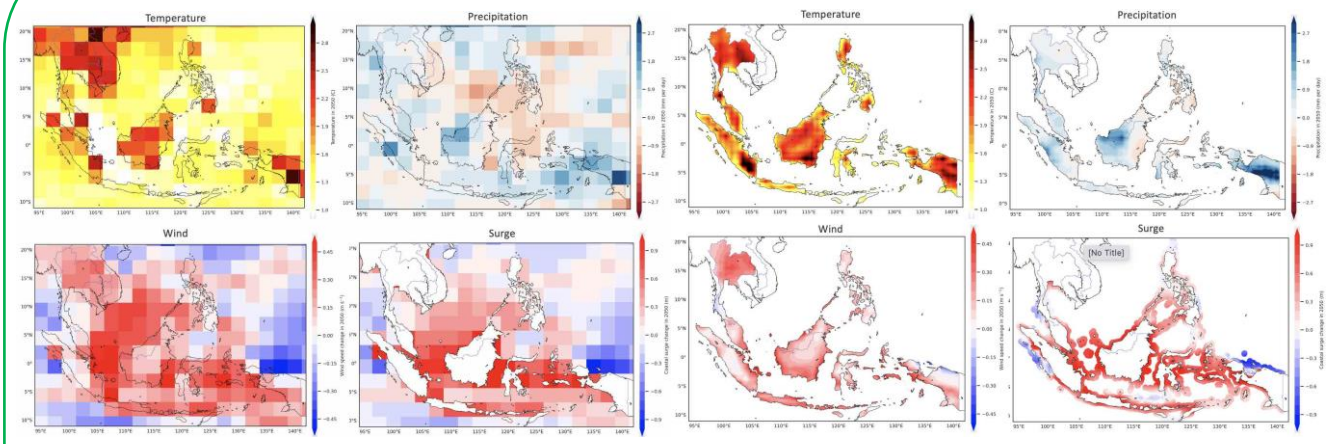

The four charts on the left use a global climate model and depict the impact of climate scenario RCP8.5-2050 on the average temperature, precipitation, windspeed and coastal surge across the geographies of interest. The charts on the right report the downscaled version of the results at a spatial resolution of 1km x 1km.

Figure B. Country risk scoring: average impact and tail risk along the RCP8.5-2050 scenario.

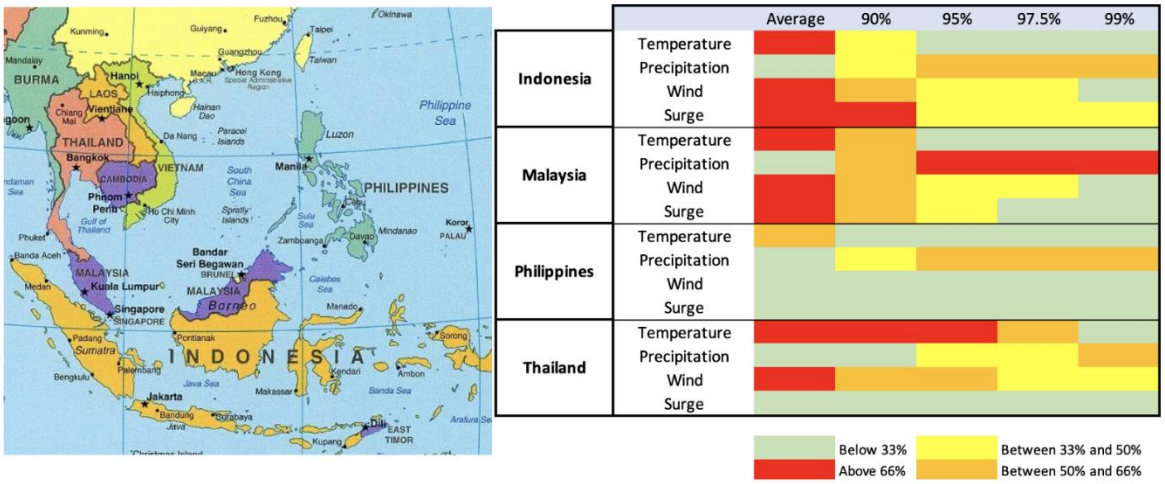

Downscaling average impact and tail risk for climate scenario RCP8.5-2050. Country based risk scores are defined based on the aerial surface experiencing sizeable changes in distribution at the average level, or at the 90-th, 95-th, 97.5-th and 99-th percentile levels. Risk scores are low (green), medium (yellow), high (orange) and severe (red), depending on the aerial surface affected by such changes.

Figure C. Downscaling at urban cluster level.

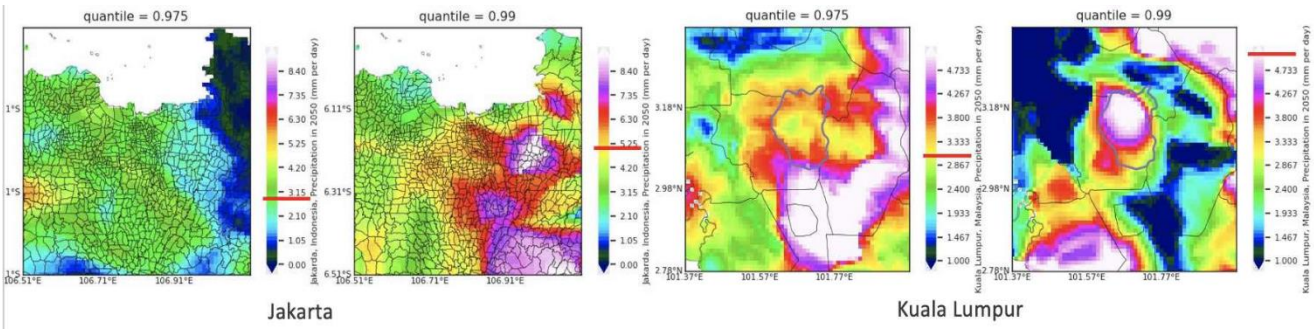

Downscaling tail risk (97.5-th and 99-th percentile) at urban cluster level. Results are reported for precipitation (in mm per day) for Jakarta (lef charts) and Kuala Lumpur (right charts). The red markers on the color scales indicate the output of a global climate model. Without downscaling, Jakarta would simply appear colored in green (97.5th percentile) or yellow (99th percentile), whereas Kuala Lumpur would appear as yellow (97.5th percentile) or white (99th percentile). The results demonstrate how material the risk of over/under-estimating risk in the absence of appropriate downscaling.

Table of Contents

1. Introduction
2. Methodology
3. Results: average impact
4. Results: tail risk
5. Results: urban clusters
6. Results: typhoon risk
7. Conclusion and next steps
8. Appendix

1. Introduction

A warm and moist atmosphere, primarily modulated by the tropical ocean, creates an ideal environment for extreme rainfall in Southeast Asia. Most countries in the region have long coastlines exposed to frequent coastal surges (of water from the ocean) as well as typhoons. The variability of rainfall patterns in Southeast Asia is quite significant due to the local monsoon systems. For instance, rainfall in Thailand and the Philippines is largely influenced by the South Asian summer monsoon creating heavy rainfall during the May-September period, whereas the boreal winter monsoon brings extreme rainfall to countries such as Singapore and Malaysia between November and March.

Global warming is associated with at least three physical risks that are relevant in SEA:

- Sea level rise, resulting from the thermal expansion of seawater and melting of land-based ice sheets and glaciers.
- Increase in precipitation, resulting from warmer air being able to hold more water vapor — with a rate of 7% per degree rise in temperature[4].
- Changes in rainfall variability associated with changes in the monsoon system in Southeast Asia[5].

Sea level rise and increase in precipitation are broadly associated with a worsening risk profile of storm surge and excess rainfall events, which can be broadly understood with global models, but require downscaling to properly gauge impact at location. Changes in rainfall variability, however, cannot be easily analyzed with global models, as they are modulated by an evolving monsoon system. This in turn makes it challenging to predict the footprint of storm surge and extreme rainfall events throughout Southeast Asia.

In this report, we look at the above challenges and show **how downscaling can inform our understanding of physical risks for climate sensitive valuations and stress testing exercises**. We study the evolution of the following climate variables along representative concentration pathway[6] (RCP) 8.5 until 2050 (henceforth referred to as **RCP8.5-2050 climate scenario**):

1. Maximum daily **temperature**, expressed in Celsius degrees.
2. Cumulative daily **precipitation**, expressed in millimeters of rain per day.
3. Daily average **wind speed**, expressed in meters per second.
4. Daily average **coastal surge** height, expressed in meters, which represents sea level surge in excess of both astronomical tides and projected sea level rise[7]. The "Technical Appendix"

[4] Ivancic, T. J., & Shaw, S. B. (2016). A US-based analysis of the ability of the Clausius-Clapeyron relationship to explain changes in extreme rainfall with changing temperature. *Journal of Geophysical Research: Atmospheres*, *121*(7), 3066-3078.
[5] See Wang S, Toumi, R. 2021, Recent migration of tropical cyclones toward coasts, *Science*, Vol: 371, Pages: 514-517.
[6] See IPCC (2019).
[7] An increase of between 0.23 and 0.24 meters is projected for the locations of interest in this study under RCP8.5 -2050. See https://sealevel.nasa.gov/ipcc-ar6-sea-level-projection-tool.

document accompanying this report outlines a simple model of coastal surge driven by the evolution of wind speed.

Figure 1 depicts the geographical area of interest. We will focus on four countries: Indonesia, Malaysia, Philippines, and Thailand.

Figure 1. Geographical areas of focus.

Importantly, we will study changes in the distribution of the variables of interest across the different locations and not just changes in average levels. Figure 2 provides a stylized representation of what the downscaling will allow us to achieve: identifying locations likely to experience a change in the mean level, the tail risk or both, the latter representing the worst situation. By tail risk we mean the increase in frequency and severity of events deemed to be rare and extreme under the current climate environment.

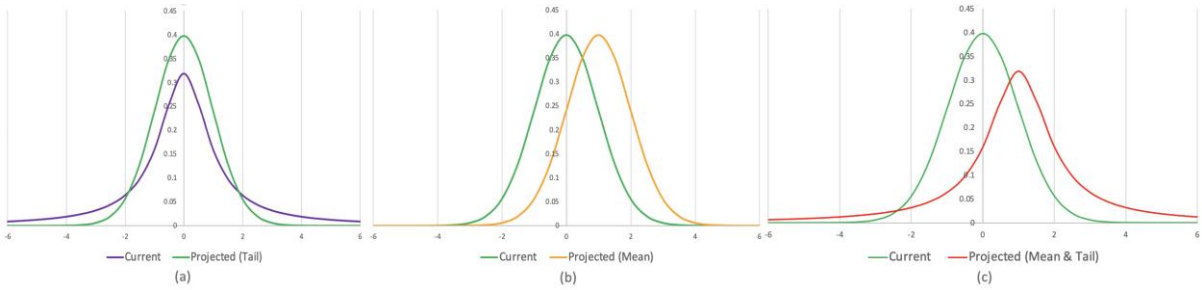

Figure 2. Changes in mean vs. tail level of a target variable. Panel (a) shows the case in which the distribution experiences a thickening of the tails in the projected climate scenario. Panel (b) shows the case of a distribution experiencing a shift in its mean level, but no changes in its tails. Panel (c) depicts a situation in which the distribution experiences both a shift in the mean level and a thickening of the tails in the projected climate scenario.

The report is organized as follows. In the next section, we provide an overview of the methodology. In section 3, we discuss downscaling results for the average level of climate variables of interest. In section 4, we will focus on tail risk and consider the 90th, 95th, 97.5th and 99th percentiles of the distribution. In section 5, we look at urban clusters to illustrate the ability of the downscaling approach to unveil considerable heterogeneity in exposures at location. Section 6 discusses some results related to typhoons, combining our understanding of the Nino/Nina effect with the footprint of typhoons in Southeast Asia. Finally, section 7 offers concluding remarks and discusses next steps. Two accompanying documents contain appendices including further results and technical information.

2. Methodology

There are two prevailing downscaling methods available in the literature:

- **Statistical approach**. It uses statistical relationships to downscale predictions at high temporal and spatial resolution. Being a reduced form approach, it is considerably efficient from a computational point of view.
- **Dynamical approach**. Its predictions rely on a structural representation of physical processes driving the phenomena of interest. As such, it can capture complex, non-linear relationships at the expense of computational tractability.

We adopt a **machine learning** approach allowing us to overcome the computational burden of the dynamical approach while at the same time uncovering interesting patterns in the spatio-temporal characteristics of relevant variables. We test four different approaches[8]:

1. Quantile Mapping (QM) method. The QM bias correction algorithm is commonly used to correct systematic distributional biases in climate model outputs. The QM model is trained by matching the cumulative distribution functions of the observed and simulated variables, and it has been widely used in climate downscaling.[9]
2. Pure Analog (best and sample analog) method. The analog approach is arguably the simplest downscaling scheme. It trains the downscaling model by associating the simulated values of a variable with the historical observations showing the greatest similarity. Because of its ease of application, the analog method has been widely applied in climate projections.[10]
3. Random Forest (RF) approach. The RF method uses advanced binary tree application based on the bagging method to add an additional layer of randomness. A decision tree is a hierarchical analysis diagram composed of a collection of nodes and edges organized in a tree structure. Use of the RF method is relatively new; see Pang et al. (2017) for an example of application to climate downscaling[11].
4. Temperature bias correction. This method was explicitly developed for temperature downscaling and usually works well in that context. We apply the same methodology to precipitation and wind speed in addition to temperature.

We use state-of-the-art global climate reanalysis data—the ERA5 data set generated by the European Centre for Medium-Range Weather Forecasts[12] —as the "observations". The future "projections" are taken from the Coupled Model Intercomparison Project (the 6th generation, CMIP-6)[13]. To train the machine learning models, we use the "simulated observations" from the CMIP6 data set. The models are trained by mapping the quantiles of each climate quantity in the "simulated observations" onto that in the "observations". The trained models are then used to bias-correct the "projections", which generate the downscaled climate scenarios for the Southeast Asian region.

---

[8] See https://www.gfdl.noaa.gov/esd_eval/.

[9] See, for example: Maraun, D. (2013), Bias correction, quantile mapping, and downscaling: Revisiting the inflation issue, *Journal of Climate*, 26(6):2137–2143; Thrasher, B., Maurer, E. P., McKellar, C., and Duffy, P. B. (2012), Bias correcting climate model simulated daily temperature extremes with quantile mapping, *Hydrology and Earth System Sciences*, 16(9):3309–3314.

[10] See, for example: Lorenz, E. N. (1969). Atmospheric predictability as revealed by naturally occurring analogues, *Journal of Atmospheric Sciences*, 26(4):636–646; Van den Dool, H. (1994), Searching for analogues, how long must we wait? *Tellus A*, 46(3):314–324.

[11] Pang, B., Yue, J., Zhao, G., and Xu, Z. (2017). Statistical downscaling of temperature with the random forest model. *Advances in Meteorology*.

[12] See Hersbach, Hans, Bill Bell, Paul Berrisford, Shoji Hirahara, András Horányi, Joaquín Muñoz-Sabater, Julien Nicolas et al. "The ERA5 global reanalysis." *Quarterly Journal of the Royal Meteorological Society* 146, no. 730 (2020): 1999-2049.

[13] See https://www.wcrp-climate.org/wgcm-cmip/wgcm-cmip6. We use the HadGEM2 model, which has a successful track record in applications to the Asian region and beyond; see Dong and Dong (2021), Evaluation of extreme precipitation over Asia in CMIP6 models, *Climate Dynamics*, 57:1751-1769.

In this report we consider a **climate scenario** following the RCP8.5 pathway until 2050. Other RCPs and longer time horizons could be considered on a demand basis, together with finer resolutions for sub-areas of interest. The four target variables of interest (temperature, precipitation, wind speed, coastal surge) are downscaled at a resolution of 1km x 1km. Precipitation, temperature and wind speed are downscaled on land, whereas coastal surge is downscaled over oceans along the coastal line, where applicable.

We choose the QM approach for our analysis based on its out-of-sample performance[14]. We find the temperature bias correction method to be the worst performer for precipitation and wind speed at our locations of interest. The analog method performs quite poorly out-of-sample for temperature and precipitation. The RF and QM methods are the two best performer, with the QM approach demonstrating considerably superior out-of-sample performance for precipitation and temperature across all quantiles. Quantile-quantile (Q-Q) plots for in-sample and out-of-sample results are reported in the companion document "Technical Appendix".

3. Results: average impact

In this section we focus on the average impact of global warming on the climate variables of interest. We consider changes in target variable (e.g, in daily maximum temperature) along RCP8.5-2050 *relative to current climatic conditions*. A positive (negative) change therefore represents an increase (decrease) in the target variable relative to current climate.

Figure 3 reports changes in the average value of each variable of interest along RCP8.5-2050. It is apparent that **Thailand** experiences rather large increases in average temperature and wind speed but is relatively shielded by increases in average precipitation and coastal surge. The latter is quite material for the southernmost coastal areas, the Andaman Sea being a notable exception, as average surge height decreases there.

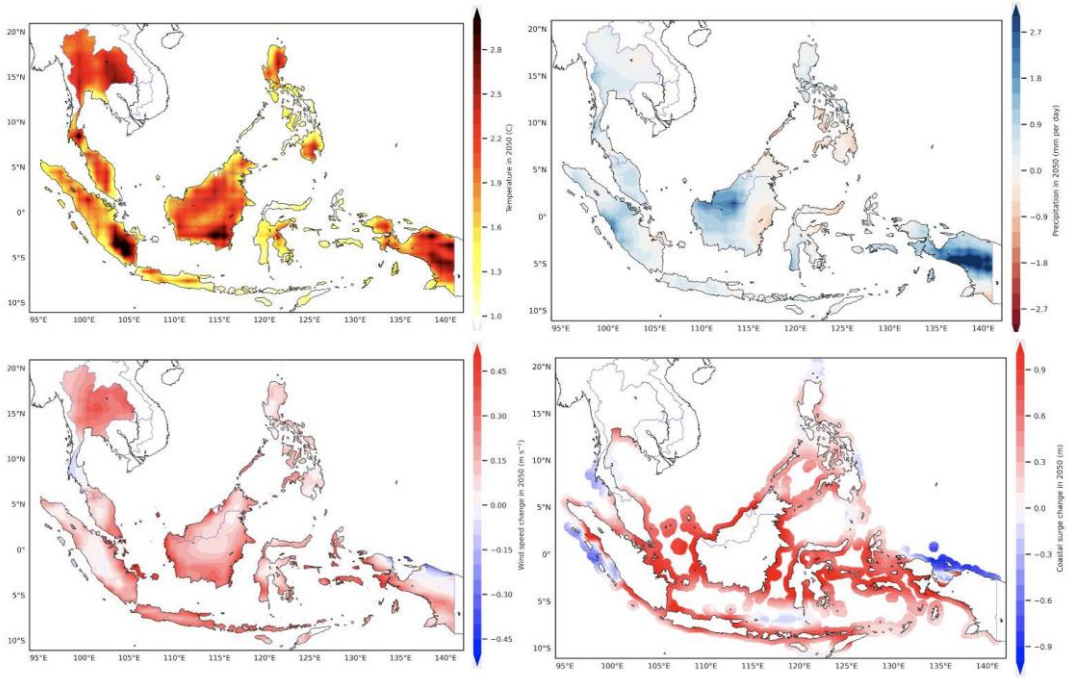

Figure 3. Global warming impact (CMIP6-implied results for the RCP 8.5 pathway until 2050) on the average level of different variables: temperature (top left), precipitation (top right), wind

[14] For a discussion of the QM method and its main features, see Gudmunsson et al. (2012) Downscaling RCM precipitation to the station scale using quantile mapping – a comparison of methods, Technical note, *Hydrology and Earth System Sciences*, 9, 6185–6201.

speed (bottom left), coastal surge (bottom right). Results are reported in terms of differences relative to current climate. Differences are in Celsius degrees for temperature, millimeters per day for precipitation, meters per second for wind speed, and meters for coastal surge.

The **Philippines** experience relatively high temperature increases in the northernmost and southernmost regions, whereas the impact on coastal surge is overall moderate, but quite relevant for the central and southwestern part of the country.

Malaysia is exposed to sizeable changes in the average level of all variables of interest. The southwestern part of the country experiences the largest increase in average precipitation.

Indonesia is also considerably affected. The most dramatic increase in temperature and wind speed is experienced in the Lampung, South and Central Kalimantan, and Papua areas. Papua is also exposed to sizeable increase in average precipitation. Average coastal surge is markedly increased throughout, except for West Sumatra and parts of West Papua.

The results depicted here provide clear **evidence of a marked shift in the average exposure to physical hazards, with important geographical differences within and across countries**. Figure 4 reports results for the differences between downscaled and CIMP-6-implied changes in average levels relative to current climate. The results demonstrate that the outputs of the global climate model provide too coarse a representation of climate risk exposures and therefore cannot enable the formulation of the predictions above.

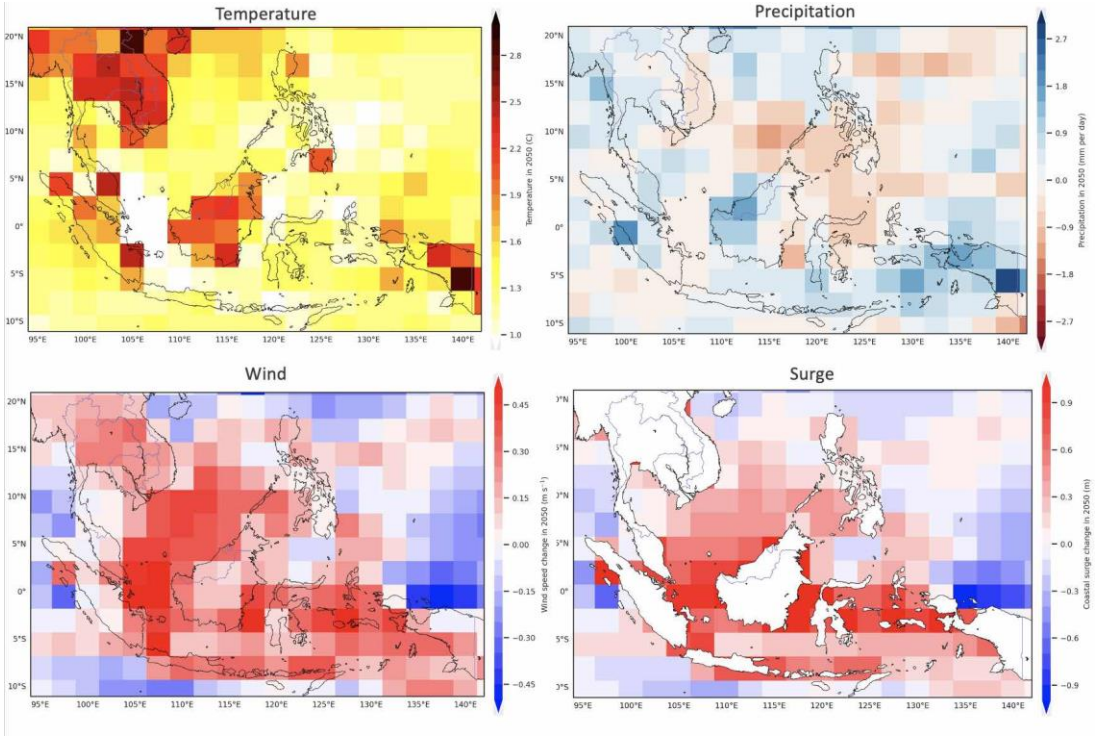

Figure 4. Global warming impact on the average level of different variables according to the CIMP-6 model (no downscaling): temperature (top left), precipitation (top right), wind speed (bottom left), coastal surge (bottom right). Results are reported in terms of differences relative to current climate. Differences are in Celsius degrees for temperature, millimeter per day for precipitation, meters per second for wind speed, and meters for coastal surge.

To compare our results across countries, we then introduce a **simple rating system** labelling changes in average target variables as being low (green), medium (yellow), high (orange) or severe (red), depending on the aerial surface of the country experiencing a large enough change in target variable. The latter is defined by specifying suitable thresholds for the change in each variable. We use the following triggers:

- Temperature: a change in daily average maximum temperature above 5% of current levels.
- Precipitation: a change in daily average cumulative rainfall above 10% of current levels.
- Wind speed: a change in daily average wind speed above 10% of current levels.
- Coastal surge: a change in daily average coastal surge height above 10% of current levels.

Choice of the first threshold is justified as follows. If the average daily maximum temperature is above 30 degrees Celsius, then a change of more than 5% relative to current levels represents an increase in temperature of more than 1.5 degrees, which is consistent with a violation of the Paris Agreement's pledge. The thresholds chosen for precipitation and wind speed are possible examples of material changes in the average risk profile. The coastal surge linear model introduced in the "Technical Appendix" document inherits the threshold chosen for wind speed.

Threshold violations are assessed for every location in the downscaled grid and aggregated across locations within each country. If **less than a third** of the country (by aerial surface) experiences a large enough increase in target variable, then that physical risk dimension is classified as **low (green)**. If **more than a third, but less than half** of the country, experiences a large enough increase in target variable, then that physical risk dimension is classified as **medium (yellow)**. If **more than a half, but less than two thirds** of the country, experiences a large enough increase in target variable, then that physical risk dimension is classified as **high (orange)**. If **more than two thirds** of the country experience a large enough increase in target variable, then that physical risk dimension is classified as **severe (red)**. Again, choice of the aerial surface thresholds is for illustrative purposes only. Clearly different thresholds could be chosen by market participants depending on their risk tolerance and the geographical footprint of their exposures.

Results of the risk scoring exercise are presented in Figure 5. They confirm severe changes in the average level of temperature, wind speed and coastal surge for Indonesia and Malaysia. Thailand is less exposed to surge height, whereas the Philippines present a high-risk score only for the temperature variable. As the analysis of the next section will reveal, the low-risk scores attracted by average precipitation mask a severe exposure to extreme rainfall events.

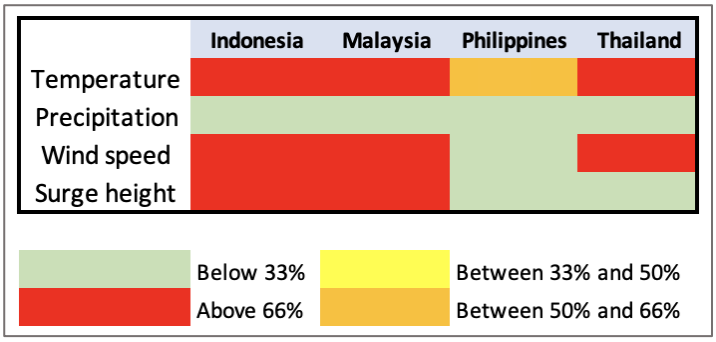

Figure 5. Risk scoring results for the impact of global warming on the average level of different variables: temperature (top left), precipitation (top right), wind speed (bottom left), coastal surge (bottom right). Results are reported in terms of difference relative to current climate. Differences are in Celsius degrees for temperature, millimeters per day for precipitation, meters per second for wind speed, and meters for coastal surge.

4. Downscaling: tail risk

In this section we focus on the results of the downscaling exercise for tail risk. We look at changes in four percentiles of the distribution of our target climate variables along RCP8.5-2050: the 90th, 95-th, 97.5-th and 99th percentiles. These are often referred to by insurers, catastrophe modelers and other data vendors as capturing 1-in-10, 1-in-20, 1-in-40 and 1-in-100 year events, respectively.

Figures 6 to 9 report results across the Southeast Asian region. Parameter values are available across locations at a resolution of 1km x 1km. Finer resolution parameters can be delivered on a demand

basis. The results show a **remarkable heterogeneity of global-warming-driven tail risk for different climate variables and locations**.

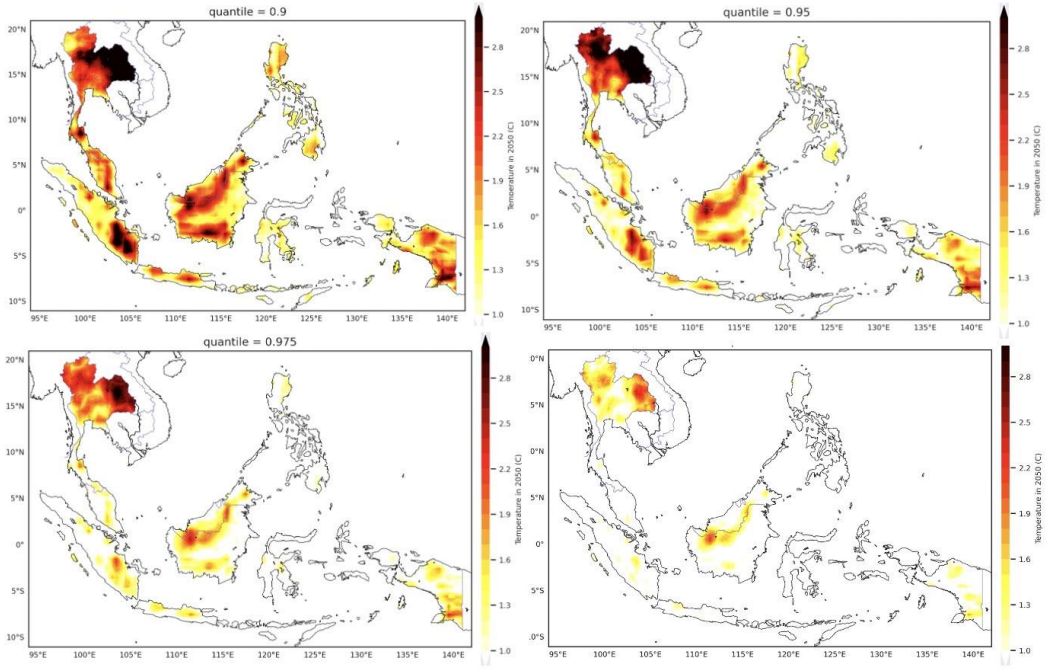

Figure 6. Impact of global warming on different temperature quantiles: 90th (top left), 95th (top right), 97.5th (bottom left), and 99th (bottom right) percentiles. Results are reported in terms of difference relative to current climate levels. Differences are in Celsius degrees.

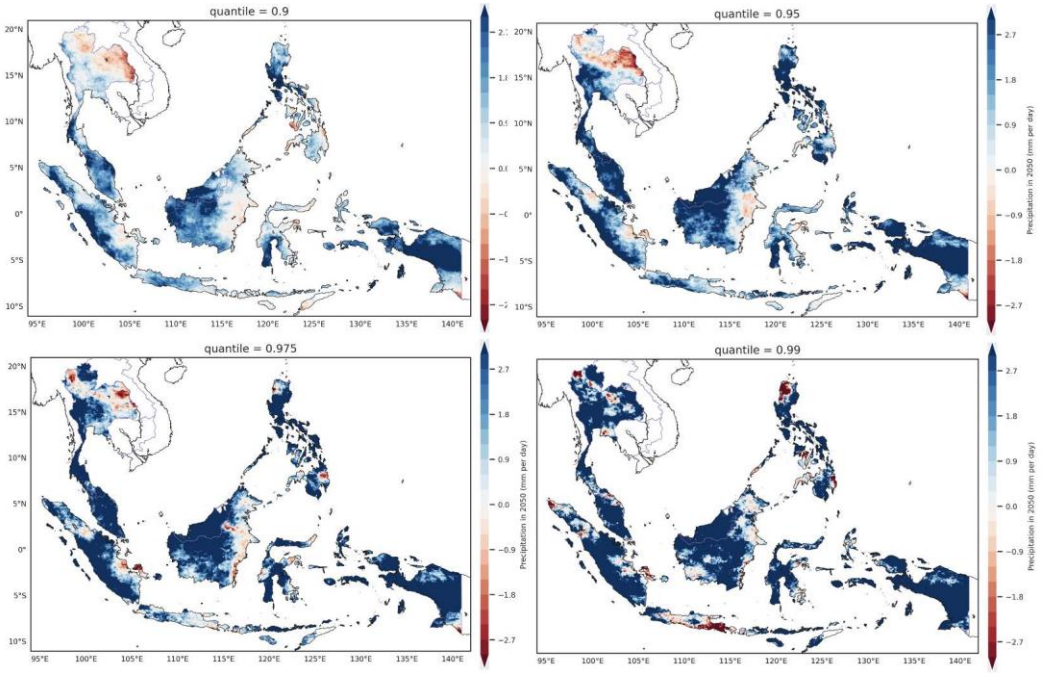

Figure 7. Impact of global warming on different precipitation quantiles: 90th (top left), 95th (top right), 97.5th (bottom left), and 99th (bottom right) percentiles. Results are reported in terms of difference relative to current climate levels. Differences are in millimeters per day.

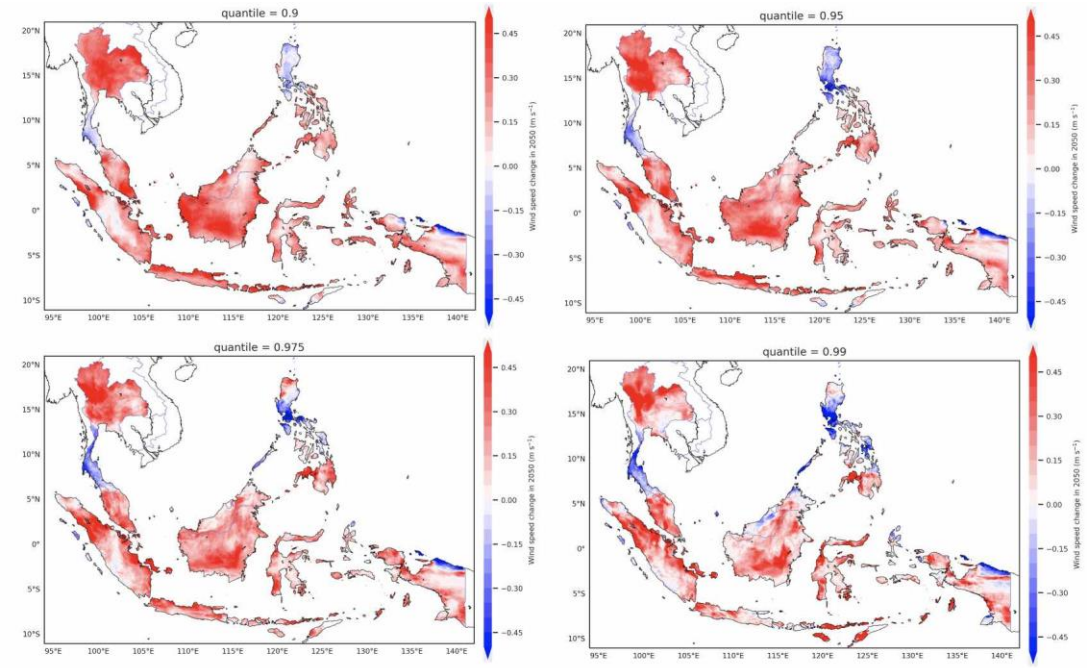

Figure 8. Impact of global warming on different wind speed quantiles: 90th (top left), 95th (top right), 97.5th (bottom left), and 99th (bottom right) percentiles. Results are reported in terms of difference relative to current climate levels. Differences are in meters per second.

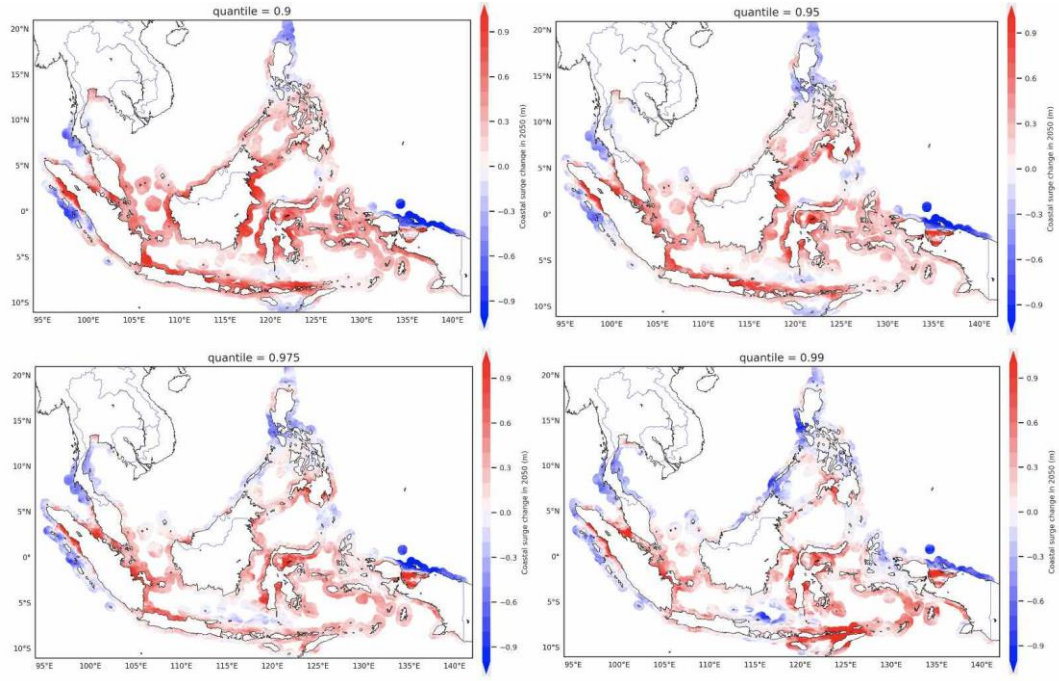

Figure 9. Impact of global warming on different costal surge quantiles: 90th (top left), 95th (top right), 97.5th (bottom left), and 99th (bottom right) percentiles. Results are reported in terms of difference relative to current climate levels. Differences are in meters.

To better visualize the overall relevance of tail risk for different countries, we adopt the risk scoring mechanism discussed in the previous section. We use the same thresholds to classify changes in tail risk as being "sizeable" and then aggregate results across locations. Again, we assign scores (low, medium, high, severe) depending on the aerial fraction of each country exposed to sizeable risk.

Figure 10 reports the results obtained for different percentiles, together with those discussed in the previous section for changes in the average level of the variables of interest. One of the most visible

results is that **the mild impact of global warming on average precipitation levels is far outweighed by sizeable tail risk across countries**, Malaysia presenting the most severe exposure to extreme rainfall events. **Extreme coastal surge events are particularly important for Indonesia and to a lesser extent for Malaysia**. Similar findings are obtained for wind speed. **Wind speed is material for Thailand both at the average and tail level**. The Philippines are relatively shielded from extreme weather events except for precipitation, which instead features a high-scoring tail risk.

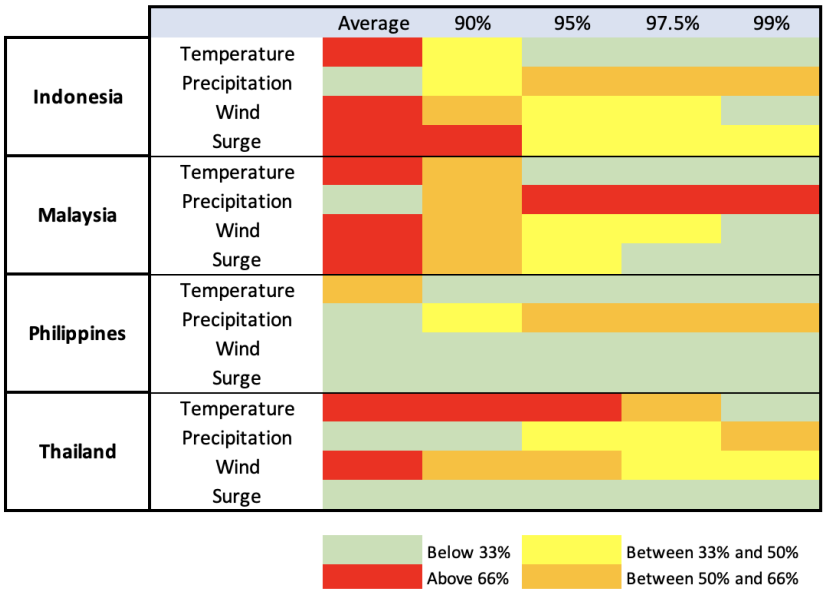

Figure 10. Impact on different costal surge quantiles: 90th (top left), 95th (top right), 97.5th (bottom left), and 99th (bottom right) percentiles. Results are reported in terms of difference relative to the CMIP6-implied results for the RCP 8.5 pathway until 2050. Differences are in meters.

5. Results: Urban clusters

In this section we look at higher resolution (500m x 500m) results for the following urban clusters[15]:

- Philippines: Manila (14.60N, 120.99E).
- Malaysia: Kuala Lumpur (3.08N, 101.67E).

We discuss some relevant examples focusing on impact on tail distribution cut-offs at the 90% and 95% percent level (90-th and 95-th percentiles).

Figures 11 and 12 provide precipitation results for Manila and Kuala Lumpur, respectively. They show **remarkable variation in tail risk across locations** and **considerable divergence relative to the outputs of the global model** (indicated by a red marker in the legend). We see that the latter would provide an overly optimistic depiction of extreme rainfall exposure through vast urban areas in the case of Manila, at both the 95th and 99th percentile levels, as well as Kuala Lumpur, at the 95th percentile level. It would instead provide an overly pessimistic depiction of extreme precipitation risk for Kuala Lumpur at the 99th percentile level. These examples offer clear evidence of the advantages of downscaling to understand the full distribution of physical risk exposures at location.

[15] A "Further Results Appendix" document complementing this report provides result for the following additional urban clusters: Bangkok, Thailand (13.76N, 100.49E); Jakarta, Indonesia (-6.21N, 106.81E).

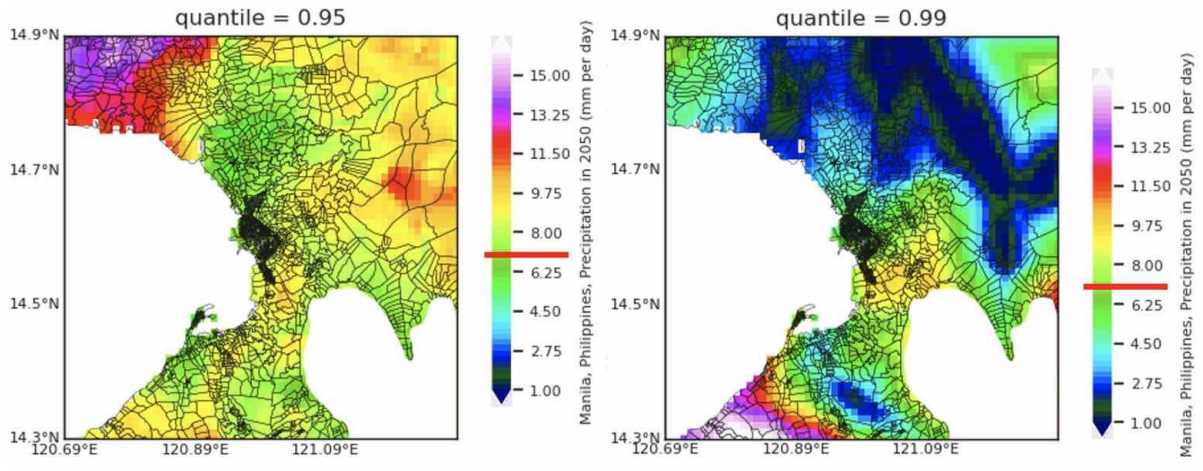

Figure 11. Precipitation impact in Manila: 95th (left) and 99th (right) percentiles. Results are reported in terms of difference between the RCP8.5-2050 scenario relative to current climate. CMIP6-implied results, which are uniform across pixels, are indicated by the red marker. Differences are in millimeters per day.

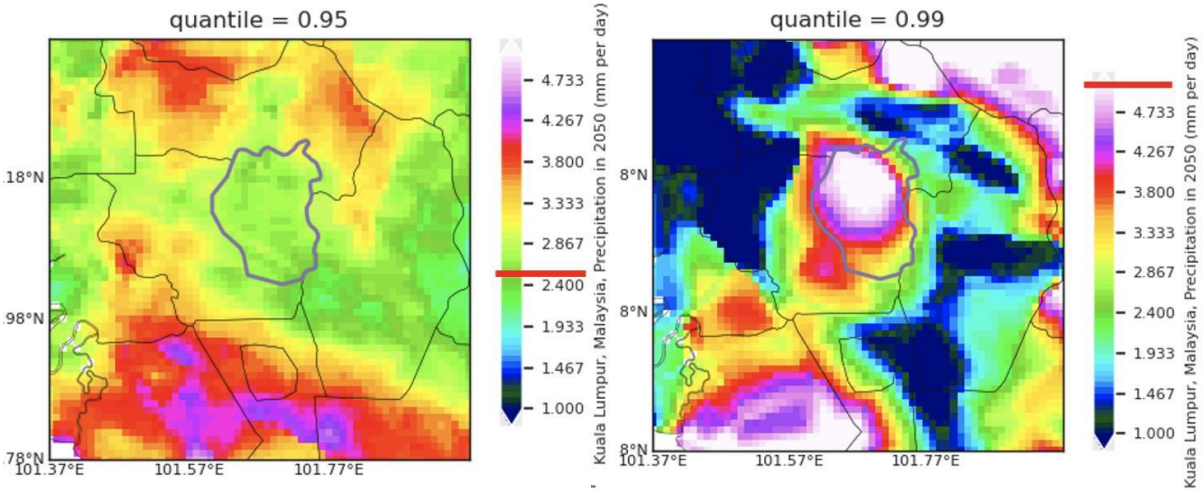

Figure 12. Precipitation impact in Kuala Lumpur: 95th (left) and 99th (right) percentiles. Results are reported in terms of differences between the RCP8.5-2050 scenario relative to current climate. CMIP6-implied results, which are uniform across pixels, are indicated by the red marker. Differences are in mm per day.

Figure 13 provides an example of downscaling results for coastal surge in Manila. We notice that appropriate, granular downscaling of the climate model suggests coastal surge is going to decrease substantially both at the 95-th and 99-th percentile levels. Importantly, the global climate model would suggest more pessimistic projections for a sizeable portion of the coastline.

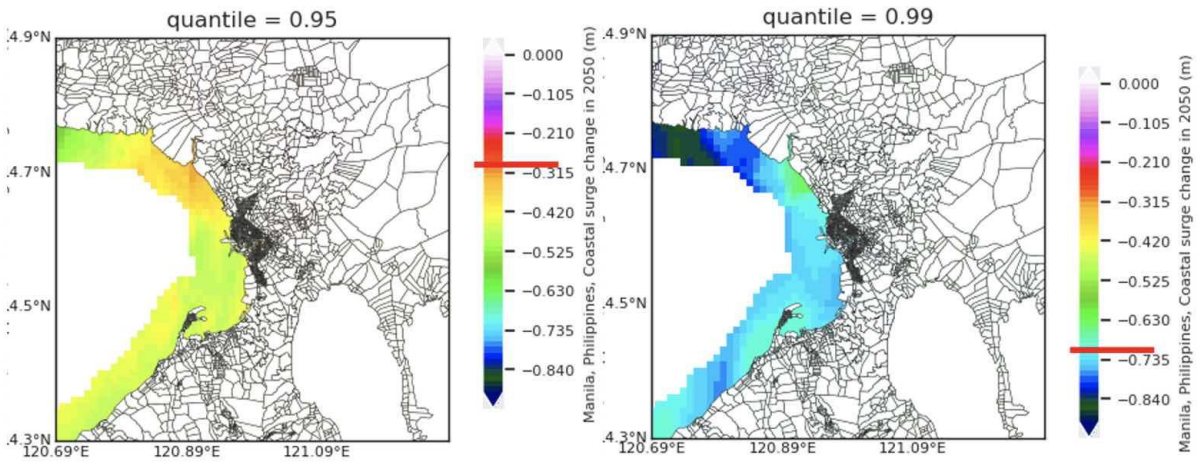

Figure 13. Coastal surge impact in Manila: 95th (left) and 99th (right) percentiles. Results are reported in terms of difference between the RCP8.5-2050 scenario relative to current climate. CMIP6-implied results, which are uniform across pixels, are indicated by the red marker. Differences are in meters.

6. Typhoon risk

We now discuss how downscaling can help understand typhoon risk in Southeast Asia, which will be addressed in future work. Here, we limit ourselves to considering the following: **i)** how typhoon risk has evolved in the past and **ii)** how the evolving variability of climate will impact typhoon activity along RCP8.5-2050.

i) It has been widely discussed in the extant literature that typhoon activity in the West Pacific area is moving polewards, suggesting a reduction in typhoon risk for relatively low latitude tropical countries[16]. Following the research community's approach to illustrating a reduced typhoon activity at low latitudes, in Figure 14 (left) we present typhoon data gridded into 4 x 4-degree latitude/longitude boxes. However, if typhoon data are gridded at a finer resolution, such as 1 x 1-degree as in Figure 14 (right), we do not see a clear reduction in typhoon activity, particularly along the Southeast Asian coastline. We therefore suggest to be cautious about claims that typhoon activity in the tropical West Pacific area has been reducing. Downscaling suggests that this is not necessarily the case for the region of interest here; recent research indeed suggests that typhoon activity there has been characterized by landward migration over the past decades[17].

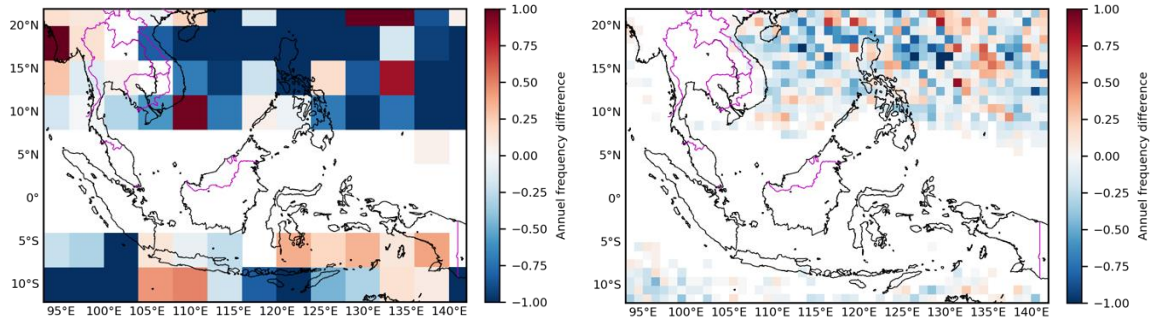

Figure 14. Historical change of typhoon activity in the SEA. The shading shows the difference between 2000-2020 and 1980-1999, with a unit of typhoon frequency per year. The left panel has

[16] Wang, S., and R. Toumi (2021). "Recent migration of tropical cyclones toward coasts." *Science* 371, no. 6528: 514-517.
[17] See Wang and Toumi (2021) and

a grid resolution of 4 degree latitude/longitude, whereas a 1 degree resolution is applied in the right panel.

ii) To study the evolution of Southeast Asian typhoon activity in future climate scenarios, we mainly focus on a climate variable recognized as being a major driver of typhoon activity: the El Niño-Southern Oscillation (ENSO) index. Changes in the index's sign characterize a regime switching behavior in typhoon activity, which shifts to the western part of the West Pacific (i.e., close to Southeast Asian countries) when the ENSO index is negative ("La Niña" regime) and toward the eastern part of the basin (i.e., away from Southeast Asian countries) when the ENSO index is positive ("El Niño" regime).

Figure 15 shows CMIP-6 based projections of the ENSO index, demonstrating that the regime switching behavior is not only likely to extend in the future, but with a more pronounced "La Niña" regimes (greater amplitude of the switch to negative index values), meaning that the shift in zonal activity may become more dramatic, with greater typhoon activity taking place in proximity of Southeast Asian countries. In summary, our results suggest an **increase in frequency and severity of typhoon activity along the climate scenario considered**. Typhoon risk will be studied extensively in later work as part of the activities of the Singapore Green Finance Centre.

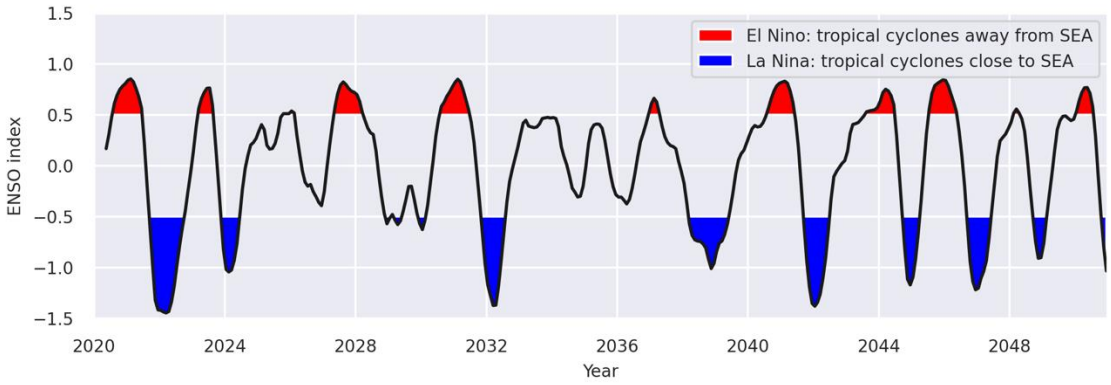

Figure 15. The El Niño-Southern Oscilation (ENSO) index for the period 2020-2050 as projected in the CMIP-6 simulations.

7. Conclusion and next steps

In this study we have demonstrated the ability of suitably chosen downscaling methods to obtain a more granular understanding of physical risk exposures at location for a group of Southeastern Asian countries of interest. We have focused on four main climate variables (temperature, precipitation, wind speed, coastal surge) and demonstrated how downscaling can reveal considerable divergence relative to the outputs of a global model both in the average level and tail distribution of target variables. We have illustrated some of our findings in relation to four urban clusters of interest (Manila and Kuala Lumpur; see the "Results Appendix" for Jakarta and Bangkok). Relevant downscaled parameters can be provided for any location of interest to market participants operating in this area. Although we have focused on spatial resolutions of 1km x 1km and 500m x 500m, our machine learning approach can deliver results at finer resolution grids at the price of greater computational effort.

There are at least three directions in which the results of this report will be further developed as part of the Climate Risk Scenario Workstream:

- Climate sensitive valuation and stress testing of various exposures/asset classes of interest (e.g., real estate, energy, sovereign risk). This will require the overlay of impact models onto the physical hazard parameters identified here.

- A deeper study of typhoon risk along different climate scenarios will be developed by Prof Ralf Toumi with the help of the Imperial College Stochastic Weather Simulator.
- Consideration of additional hazards as part of the downscaling exercise, including floods, drought and wildfires.

Two additional documents complement this report:

- A "Results Appendix" providing further outputs for urban clusters of interest.
- A "Technical Appendix" providing additional information on the downscaling methodology and its performance both in-sample and out-of-sample relative to competing methods. This document also contains details on the coastal surge model used in this report.

DOWNSCALING OF PHYSICAL RISKS FOR CLIMATE SCENARIO DESIGN

Results Appendix

Enrico Biffis[1] and Shuai Wang[2]

We provide further results for the urban clusters of interest partially discussed in section 5 of the main report:

- Philippines: Manila.
- Malaysia: Kuala Lumpur.
- Jakarta, Indonesia.
- Bangkok, Thailand.

We consider the 90-th, 95-th, 97.5-th and 99th percentiles of projected temperature, precipitation, wind speed and coastal surge at a resolution of 500m x 500m.

8.1 Manila[3] (Philippines)

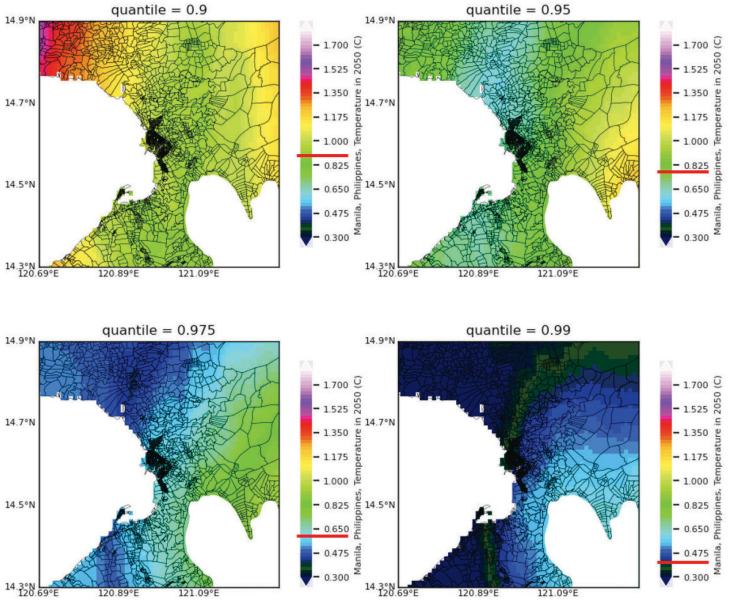

Figure 8.2.1. Maximum daily temperature impact in Manila: 90th (top left), 95th (top right), 97.5th (bottom left), and 99th (bottom right) percentile. Results are reported in terms of difference for the RCP8.5-2050 scenario relative to current climate. CMIP6-implied results, which are uniform across pixels, are indicated by the red marker. Differences are in Celsius degrees.

[1] Department of Finance and Brevan Howard Centre for Financial Analysis, Imperial College Business School; Sustainable Tech Lab at I-X, Imperial College London.
[2] Department of Civil and Environmental Engineering, Princeton University.
[3] Coordinates of the centre of the urban cluster: 14.60N, 120.99E.

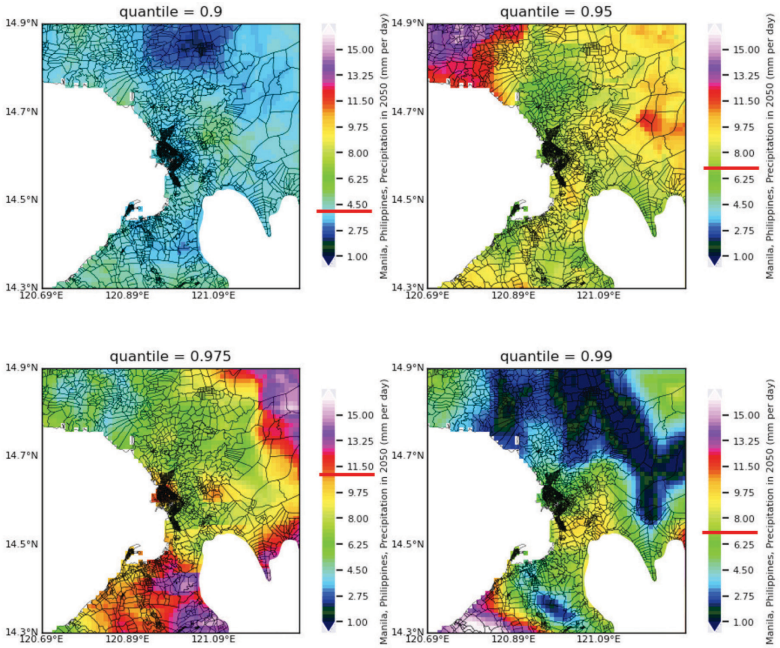

Figure 8.2.2. Cumulative daily precipitation impact in Manila: 90th (top left), 95th (top right), 97.5th (bottom left), and 99th (bottom right) percentile. Results are reported in terms of difference for the RCP 8.5 pathway until 2050 relative to current climate. CMIP6-implied results, which are uniform across pixels, are indicated by the red marker. Differences are in millimeters per day.

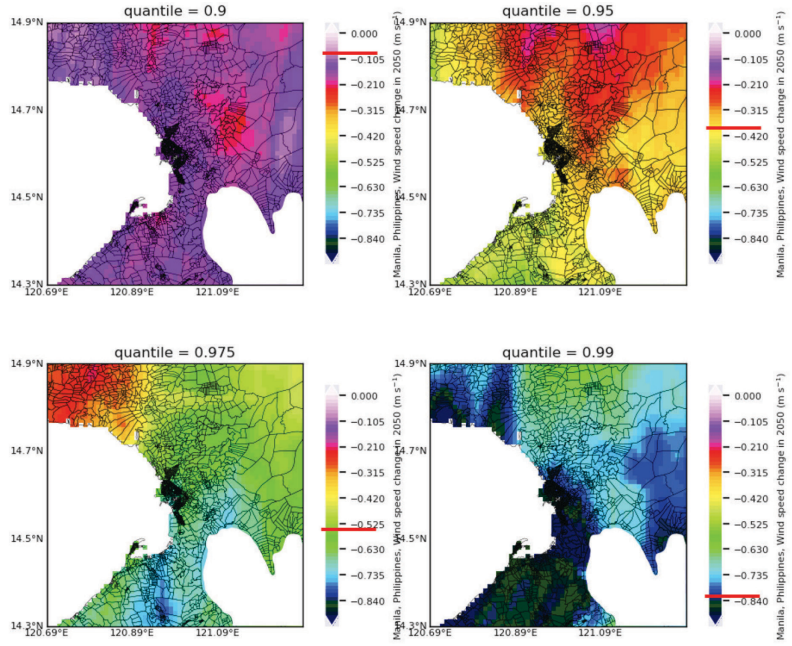

Figure 8.2.3. Daily average wind speed impact in Manila: 90th (top left), 95th (top right), 97.5th (bottom left), and 99th (bottom right) percentile. Results are reported in terms of difference for the RCP 8.5 pathway until 2050 relative to current climate. CMIP6-implied results, which are uniform across pixels, are indicated by the red marker. Differences are in meters per second.

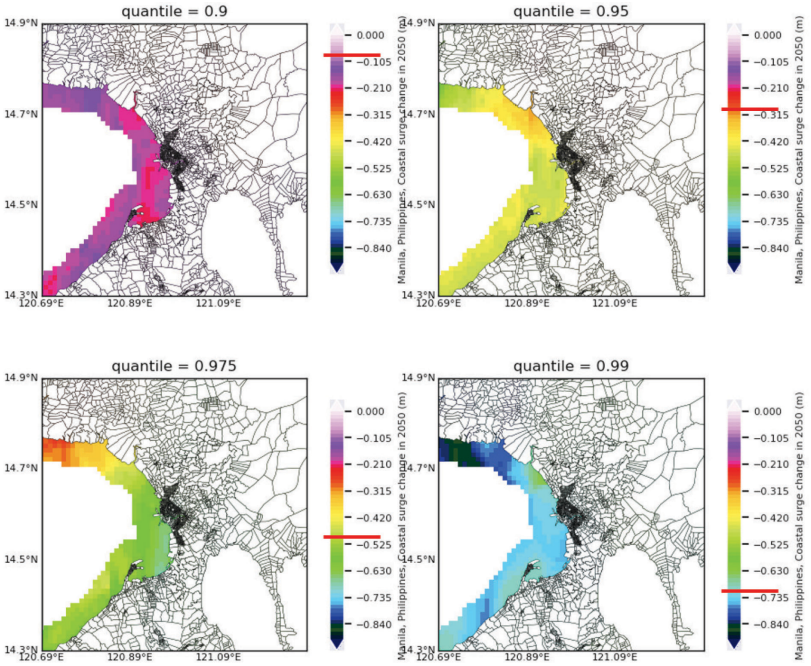

Figure 8.2.4. Daily average coastal surge impact in Manila: 90th (top left), 95th (top right), 97.5th (bottom left), and 99th (bottom right) percentile. Results are reported in terms of difference for the RCP 8.5 pathway until 2050 relative to current climate. CMIP6-implied results, which are uniform across pixels, are indicated by the red marker. Differences are in meters.

8.2 Kuala Lumpur[4] (Malaysia)

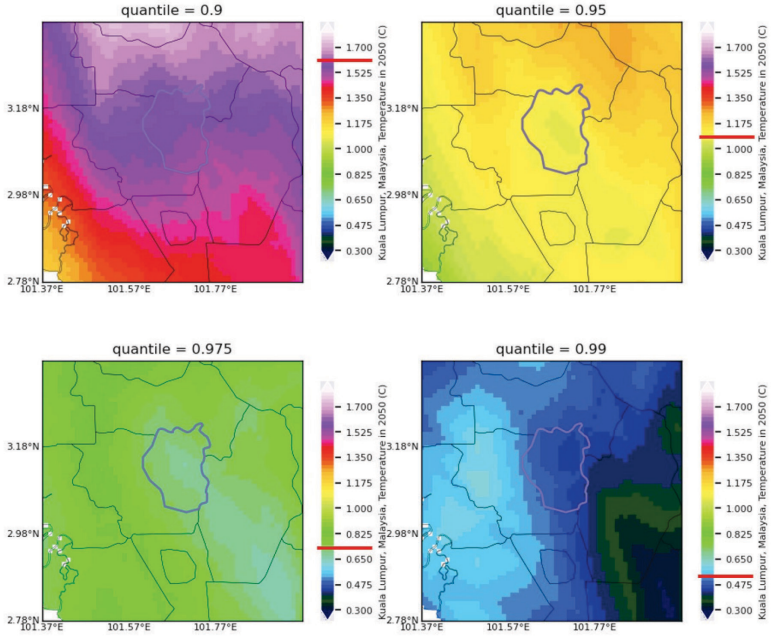

Figure 8.3.1. Maximum daily temperature impact in Kuala Lumpur: 90th (top left), 95th (top right), 97.5th (bottom left), and 99th (bottom right) percentile. Results are reported in terms of difference for the RCP 8.5 pathway until 2050 relative to current climate. CMIP6-implied results, which are uniform across pixels, are indicated by the red marker. Differences are in Celsius degrees.

[4] Coordinates of the centre of the urban cluster: 3.08N, 101.67E.

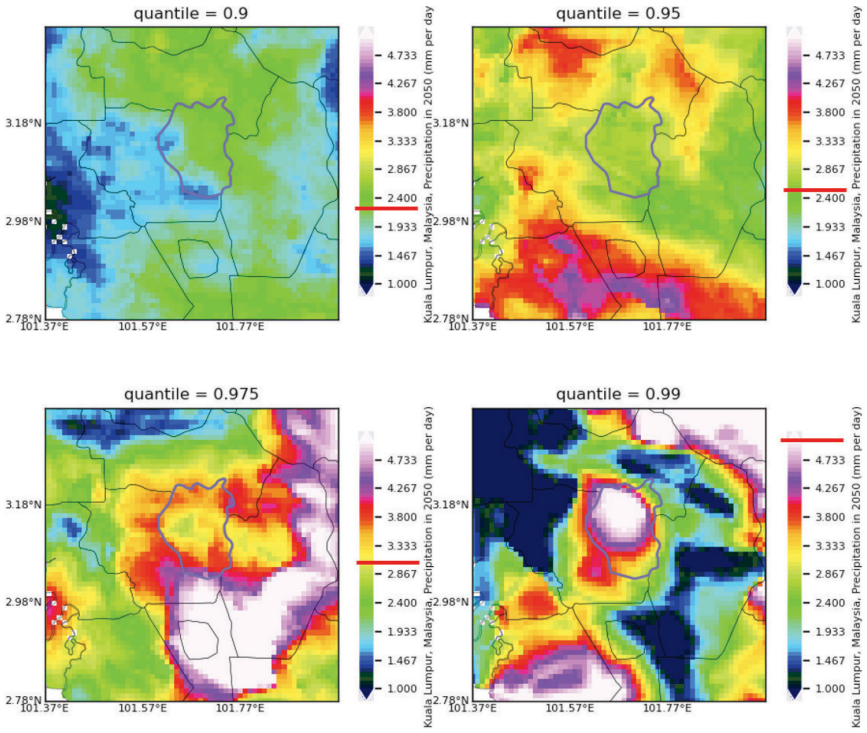

Figure 8.3.2. Cumulative daily precipitation impact in Kuala Lumpur: 90th (top left), 95th (top right), 97.5th (bottom left), and 99th (bottom right) percentile. Results are reported in terms of difference for the RCP 8.5 pathway until 2050 relative to current climate. CMIP6-implied results, which are uniform across pixels, are indicated by the red marker. Differences are in millimeters per day.

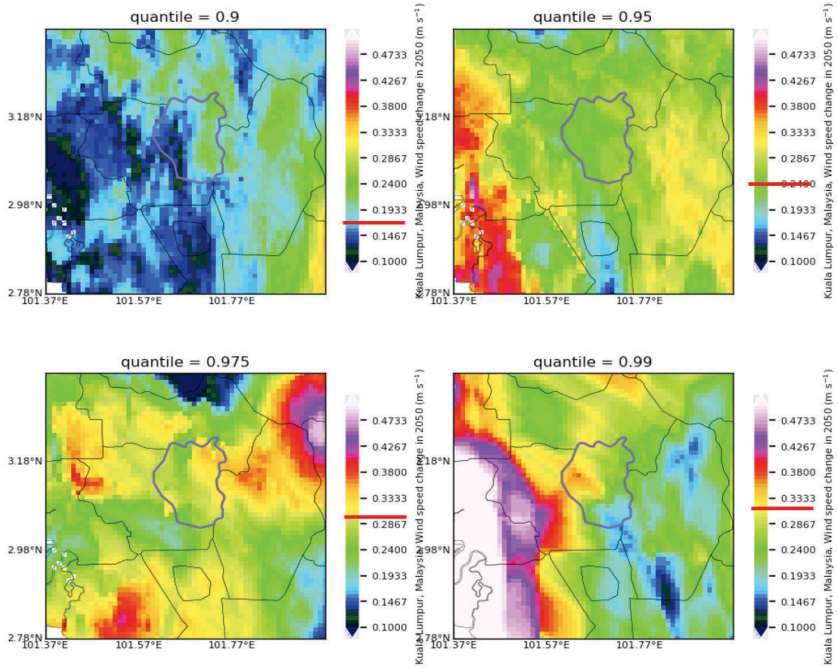

Figure 8.3.3. Daily average wind speed impact in Kuala Lumpur: 90th (top left), 95th (top right), 97.5th (bottom left), and 99th (bottom right) percentile. Results are reported in terms of difference for the RCP 8.5 pathway until 2050 relative to current climate. CMIP6-implied results, which are uniform across pixels, are indicated by the red marker. Differences are in meters per second.

8.3 Bangkok[5] (Thailand)

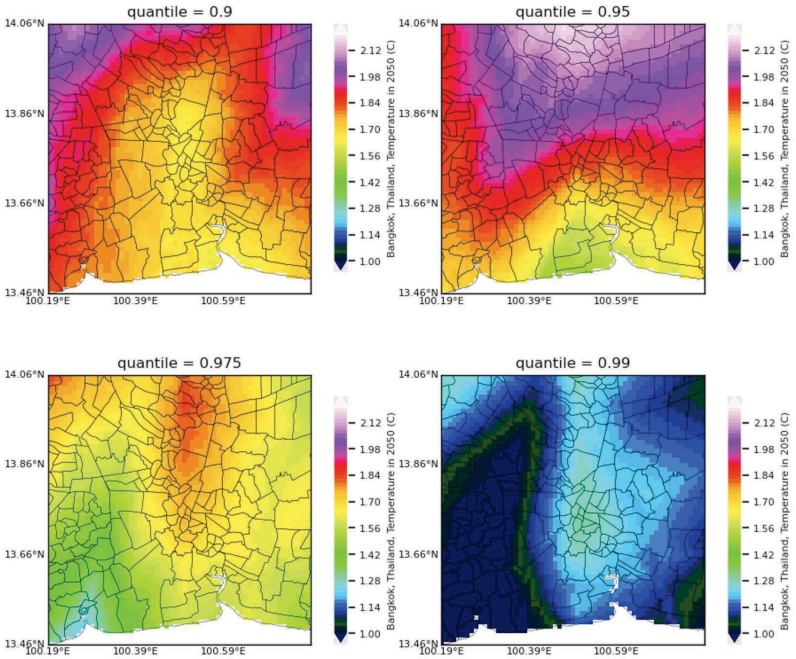

Figure 8.4.1. Maximum daily temperature impact in Bangkok: 90th (top left), 95th (top right), 97.5th (bottom left), and 99th (bottom right) percentile. Results are reported in terms of difference for the RCP 8.5 pathway until 2050 relative to current climate. CMIP6-implied results, which are uniform across pixels, are indicated by the red marker. Differences are in Celsius degrees.

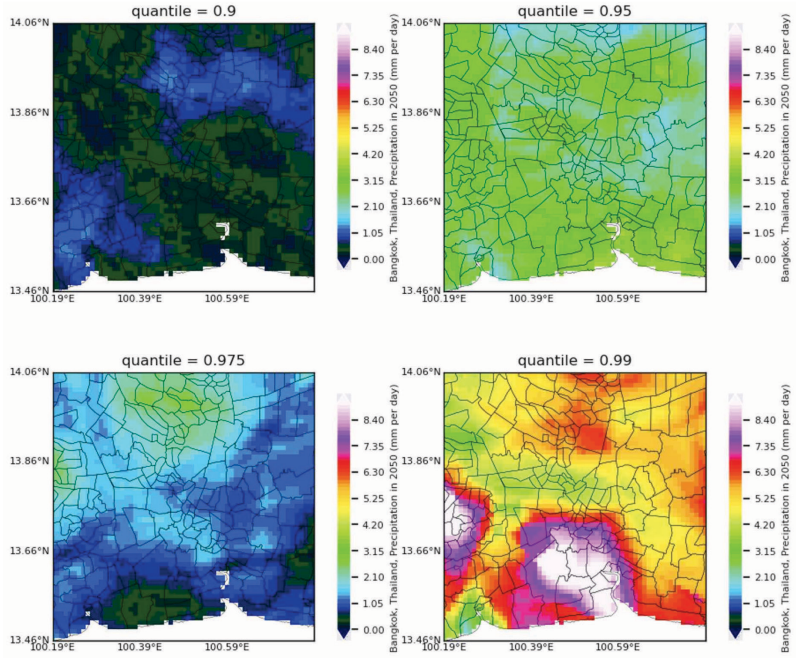

Figure 8.4.2. Cumulative daily precipitation impact in Bangkok: 90th (top left), 95th (top right), 97.5th (bottom left), and 99th (bottom right) percentile. Results are reported in terms of difference for the RCP 8.5 pathway until 2050 relative to current climate. CMIP6-implied results,

[5] Coordinates of the centre of the urban cluster: 13.76N, 100.49E.

which are uniform across pixels, are indicated by the red marker. Differences are in millimeters per day.

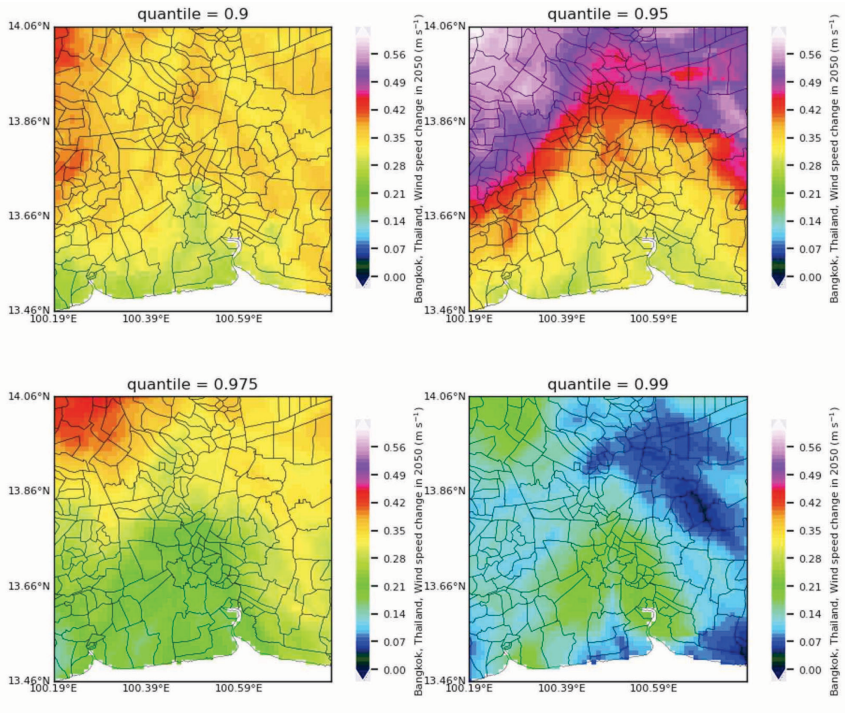

Figure 8.4.3. Daily average wind speed impact in Bangkok: 90th (top left), 95th (top right), 97.5th (bottom left), and 99th (bottom right) percentile. Results are reported in terms of difference for the RCP 8.5 pathway until 2050 relative to current climate. CMIP6-implied results, which are uniform across pixels, are indicated by the red marker. Differences are in meters per second.

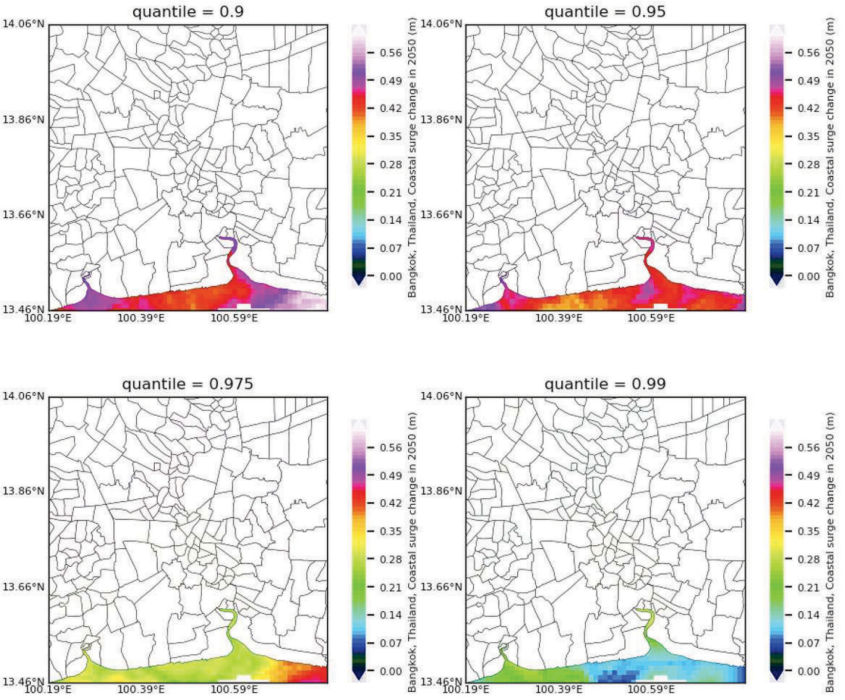

Figure 8.4.4. Daily average coastal surge impact in Bangkok: 90th (top left), 95th (top right), 97.5th (bottom left), and 99th (bottom right) percentile. Results are reported in terms of difference for the RCP 8.5 pathway until 2050 relative to current climate. CMIP6-implied results, which are uniform across pixels, are indicated by the red marker. Differences are in meters.

8.5 Jakarta[6] (Indonesia)

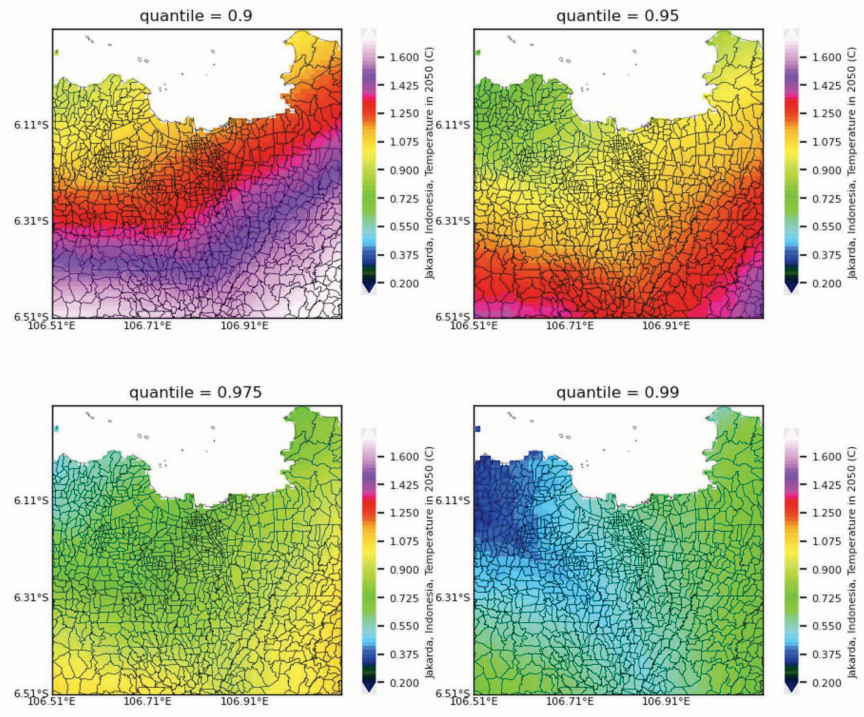

Figure 8.5.1. Maximum daily temperature impact in Jakarta: 90th (top left), 95th (top right), 97.5th (bottom left), and 99th (bottom right) percentile. Results are reported in terms of difference for the RCP 8.5 pathway until 2050 relative to current climate. CMIP6-implied results, which are uniform across pixels, are indicated by the red marker. Differences are in Celsius degrees.

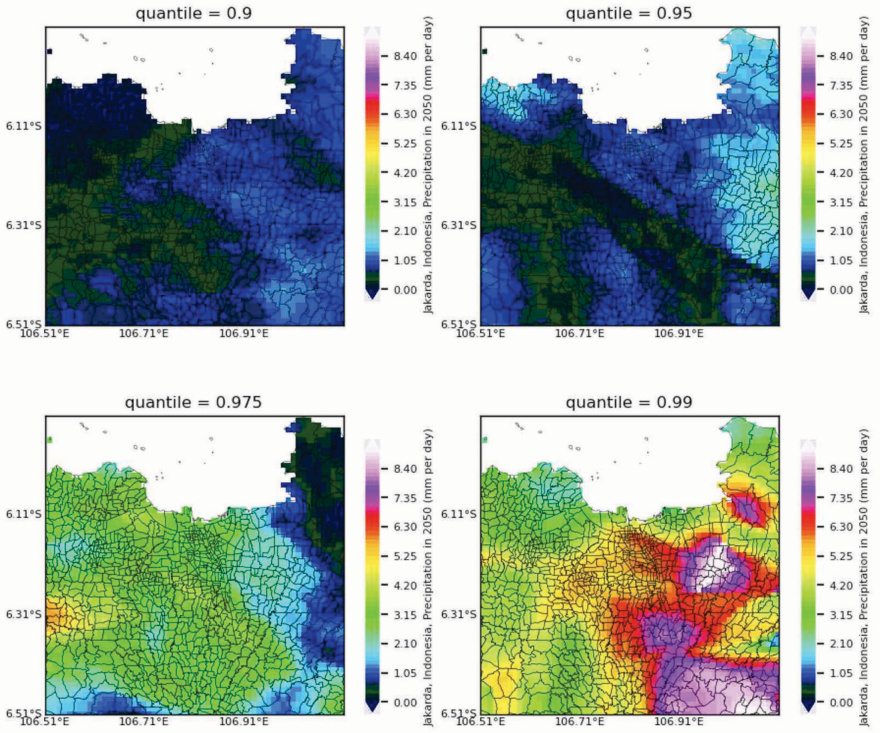

Figure 8.5.2. Cumulative daily precipitation impact in Jakarta: 90th (top left), 95th (top right), 97.5th (bottom left), and 99th (bottom right) percentile. Results are reported in terms of

[6] Coordinates of the centre of the urban cluster: -6.21N, 106.81E.

difference for the RCP 8.5 pathway until 2050 relative to current climate. CMIP6-implied results, which are uniform across pixels, are indicated by the red marker. Differences are in millimeters per day.

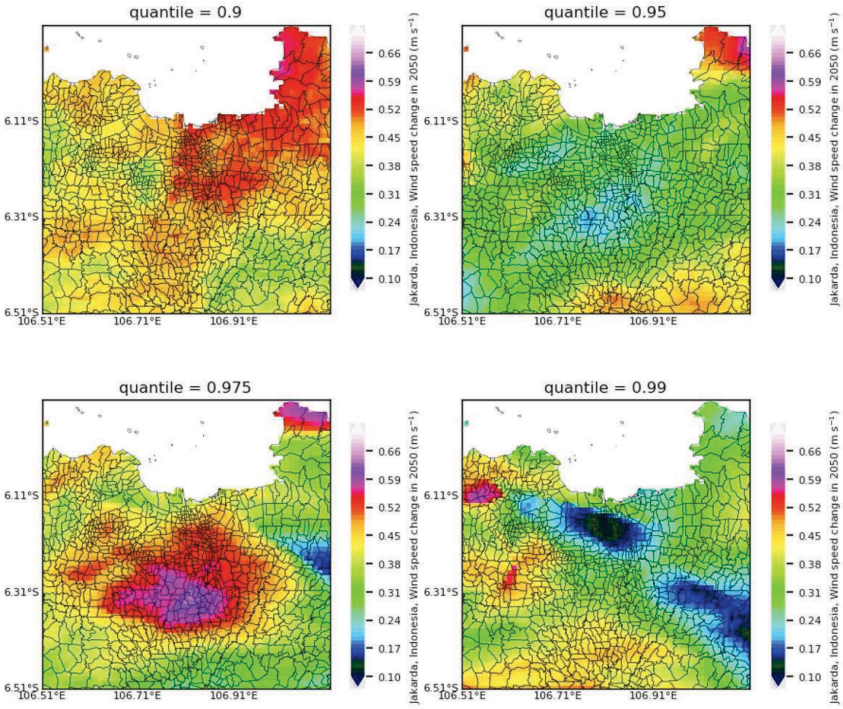

Figure 8.5.3. Daily average wind speed impact in Jakarta: 90th (top left), 95th (top right), 97.5th (bottom left), and 99th (bottom right) percentile. Results are reported in terms of difference for the RCP 8.5 pathway until 2050 relative to current climate. CMIP6-implied results, which are uniform across pixels, are indicated by the red marker. Differences are in meters per second.

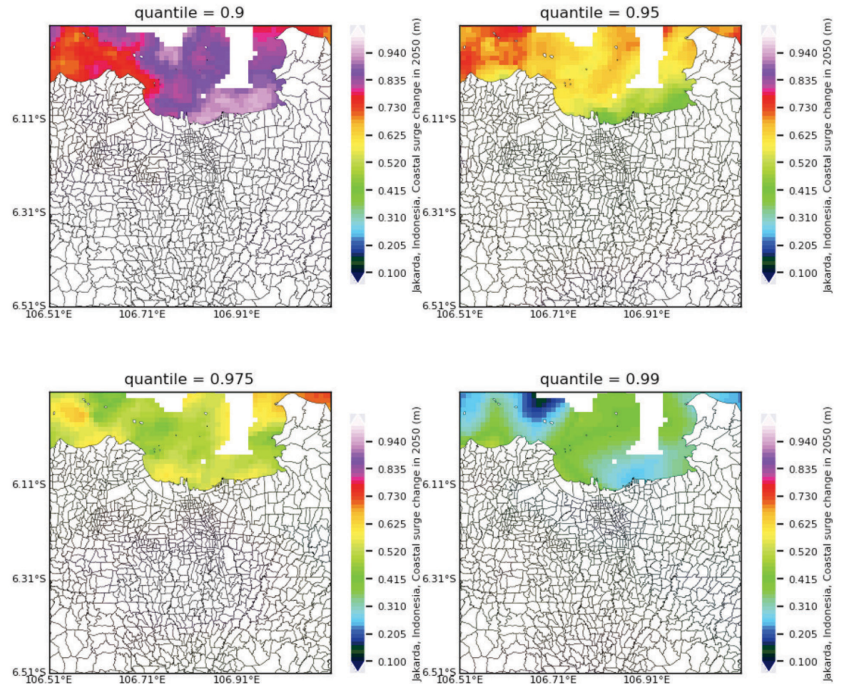

Figure 8.5.4. Daily average coastal surge impact in Jakarta: 90th (top left), 95th (top right), 97.5th (bottom left), and 99th (bottom right) percentile. Results are reported in terms of difference for the RCP 8.5 pathway until 2050 relative to current climate. CMIP6-implied results, which are uniform across pixels, are indicated by the red marker. Differences are in meters.

Downscaling of Physical Risks for Climate Scenario Design

Technical Appendix*

Enrico Biffis† Shuai Wang‡

1 Introduction

This document complements the SGFC report "Downscaling of Physical Risks for Climate Scenario Design". It provides further details on data sources, global climate model, downscaling methodology and the coastal surge model used in the report.

2 Data

We use state-of-the-art global climate reanalysis data, i.e., the ERA5 data set generated by the European Centre for Medium-Range Weather Forecasts, as the 'observations'. The ERA5 data is originally archived every 6 hours with a horizontal grid space of about 50 km. Future climate 'projections' are generated by the UK Met Office HadGEM2 model as a part of the Coupled Model Intercomparison Project (the 6th generation, CMIP-6). The CIMP-6 models can provide daily simulation outputs with a typical spatial resolution of more than 100 km. This is why the downscaling technology outlined in the next section is needed.

For climate projections, we focus on the shared socio-economic pathway (SSP) 585, which represents the high end of plausible future pathway. SSP585 is the pathway with emissions high enough to produce the 8.5 W m^{-2} level of forcing in 2100, consistent with RCP8.5. SSP585 is chosen here as it may be relatively more informative regarding the adverse climate scenario. To provide some context relative to other pathways, in figure 1 we provide the global surface temperature change to 2100 implied by five different pathways, including SSP585.

*This appendix is part of the accompanying material for the report Biffis and Wang (2022), Downscaling of Physical Risks for Climate Scenario Design, Singapore Green Finance Centre.

†Imperial College Business School.

‡Princeton University.

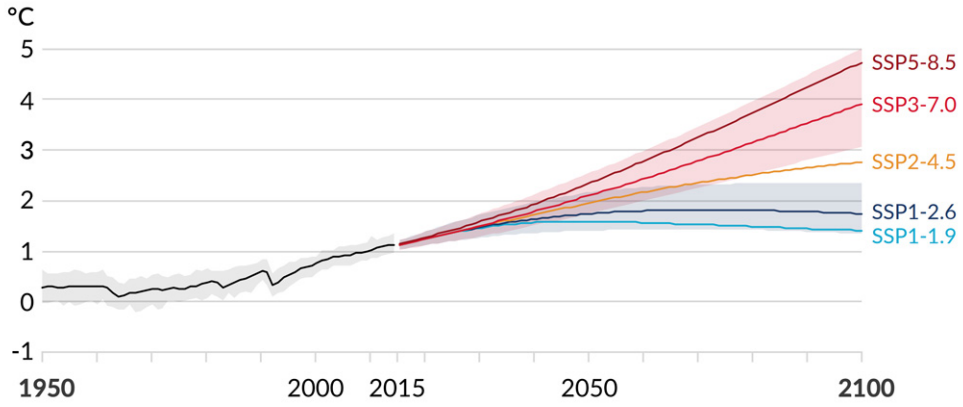

Figure 1: Global surface temperature changes relative to 1850-1900, degrees C, under the five core emissions scenarios used in AR6. Source: IPCC AR6 report Figure SPM.8a.

3 Downscaling methodologies

To train the downscaling models, we use the 'simulated observations' from the CMIP6 data set.[1] Downscaling can be carried out in multiple ways. We considered the following approaches: Quantile Mapping (QM), Pure analog (best-analog and sample-analog), Random Forest and bias correction developed for temperature simulations. The QM bias correction algorithm is commonly used to correct systematic distributional biases in climate model outputs and has been widely employed for climate downscaling (e.g., Panofsky and Brier, 1968; Maraun, 2013; Thrasher et al., 2012). The QM model is trained by equating the cumulative distribution functions of the observed and simulated variables. The analog approach is arguably the simplest downscaling scheme that trains the downscaling model by associating the simulated values of a variable with the historical observations showing the largest similarity. Because of its ease of application, the analog method has also been extensively applied in climate projections (e.g., Lorenz, 1969; Van den Dool, 1994). The random forest approach is an advanced binary tree application based on the bagging method to add an additional layer of randomness. A decision tree is a hierarchical analysis diagram composed of a collection of nodes and edges organized in a tree structure. The random forest method is relatively new but has also been used for climate downscaling (e.g., Pang et al., 2017)). The temperature bias correction method was explicitly developed for temperature downscaling achieving outstanding performance in that task.

The models were trained by mapping the quantiles of each climate quantity in the 'simulated observations' onto that in the 'observations'. The trained models were then used to bias-correct the 'projections', which generate the downscaled climate scenarios for the Southeast Asian region. Application of the temperature bias correction method to precipitation and wind speed was found to perform considerably more poorly than the other methods considered here. The temperature bias correction method was therefore ruled out first. The other methods were compared based

[1]The python downscaling package is publicly available at: https://scikit-downscale.readthedocs.io/en/latest/

on both in-sample and out-of-sample performance across the entire distribution. The quantile-quantile (Q-Q) plot results shown in Figures 2-7 demonstrate the superiority of the QM approach relative to the others, in particular when looking at the tails of the the climate variables of interest.

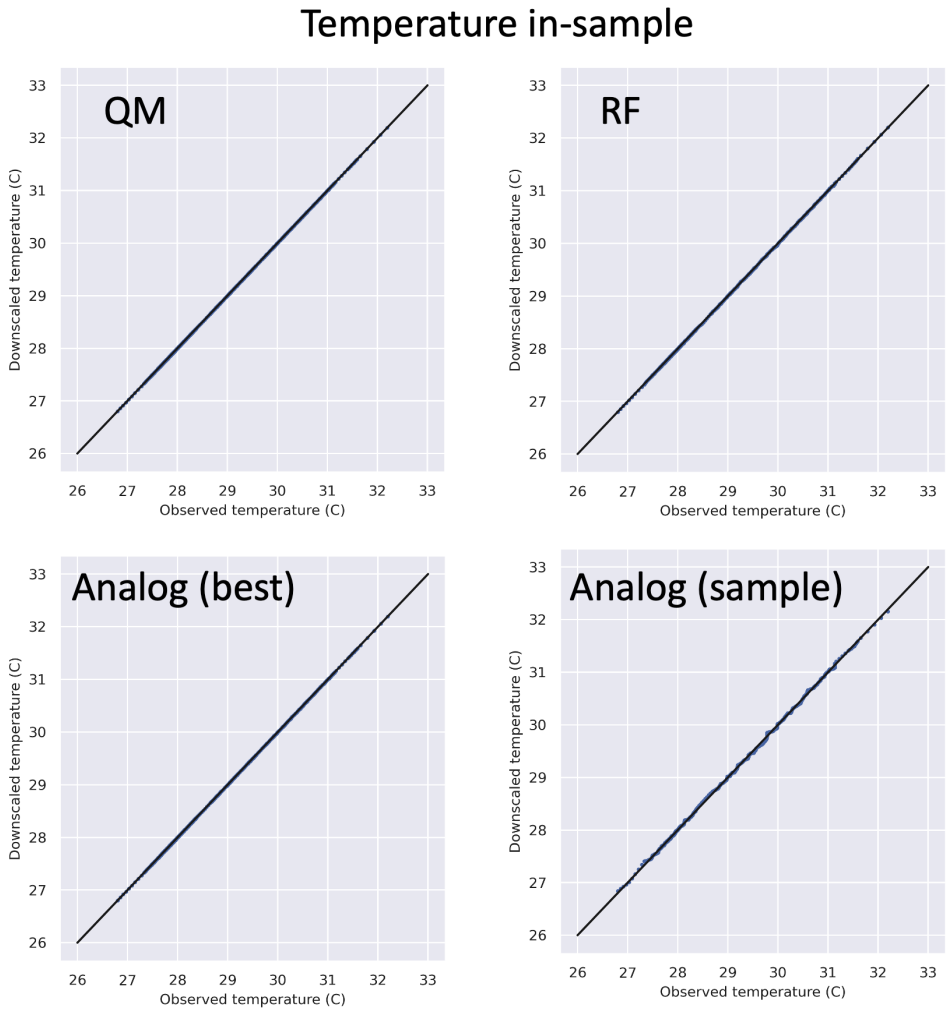

Figure 2: Q-Q plot of **in-sample temperature** comparison with different downscaling methods: quantile mapping (upper-left), random forest (upper-right), best analog (bottom-left), sample-analog (bottom-right) . Each dot represents the daily averaged value for Malaysia.

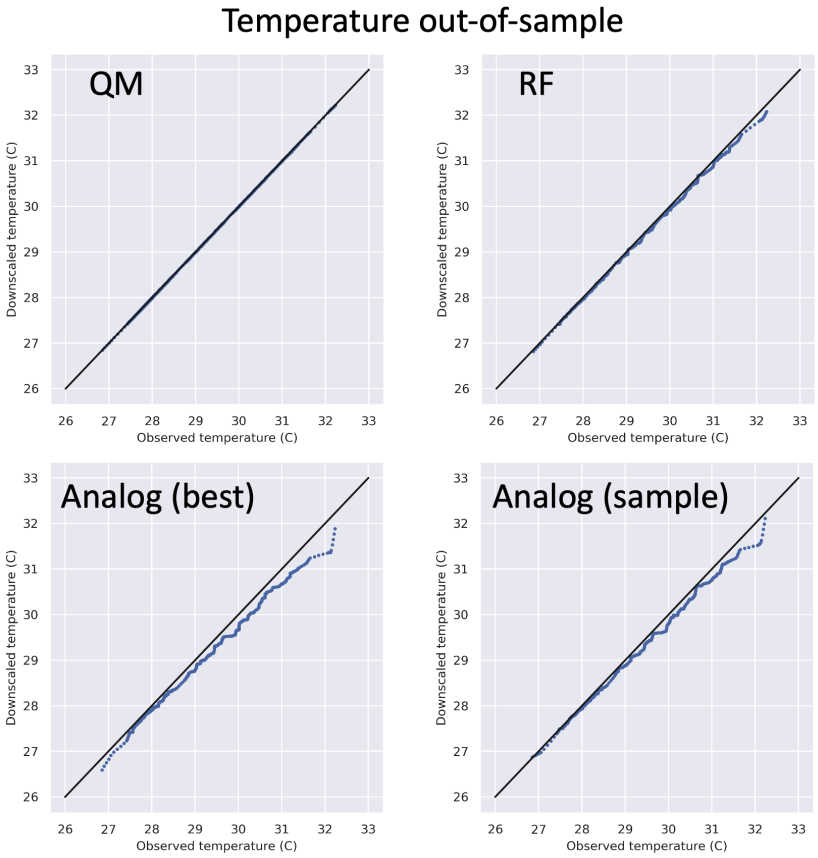

Figure 3: Q-Q plot of **out-of-sample** maximum daily **temperature** comparison with different downscaling methods: quantile mapping (upper-left), random forest (upper-right), best analog (bottom-left), sample-analog (bottom-right) . Each dot represents the daily averaged value for Malaysia.

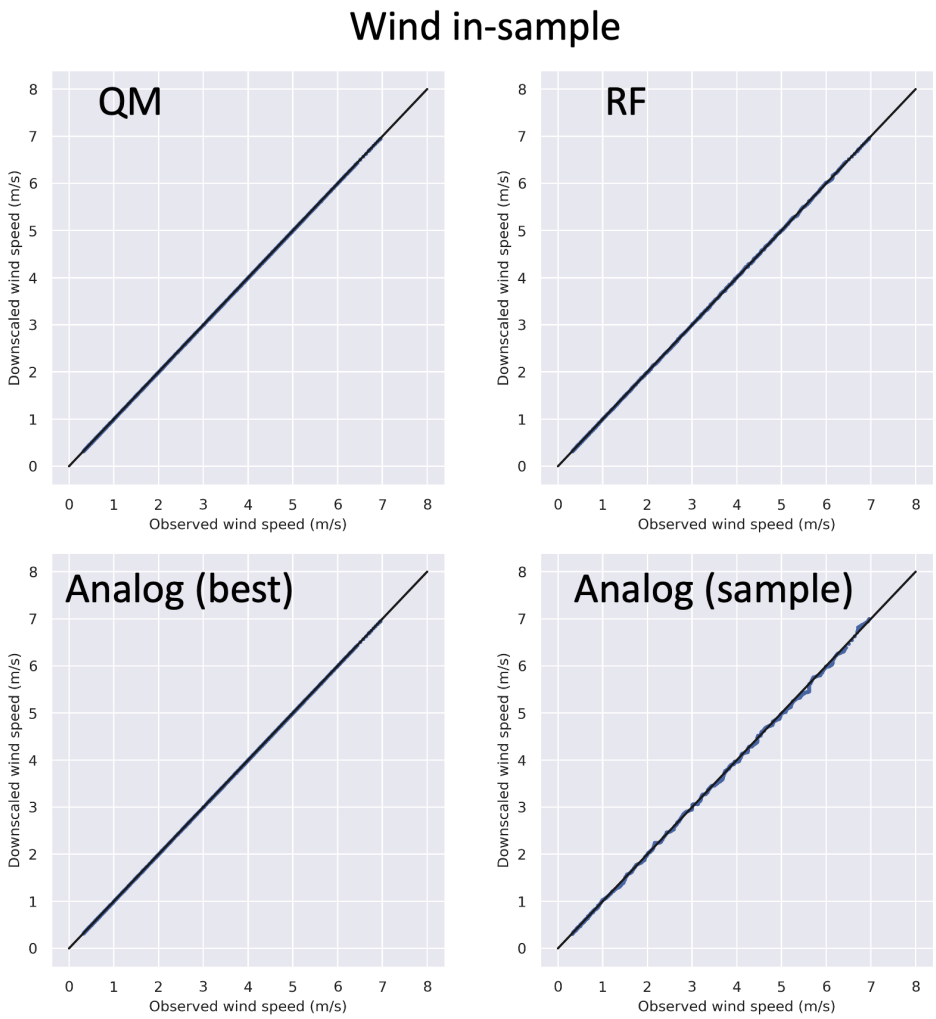

Figure 4: As in Figure 2, but for daily average **wind speed**.

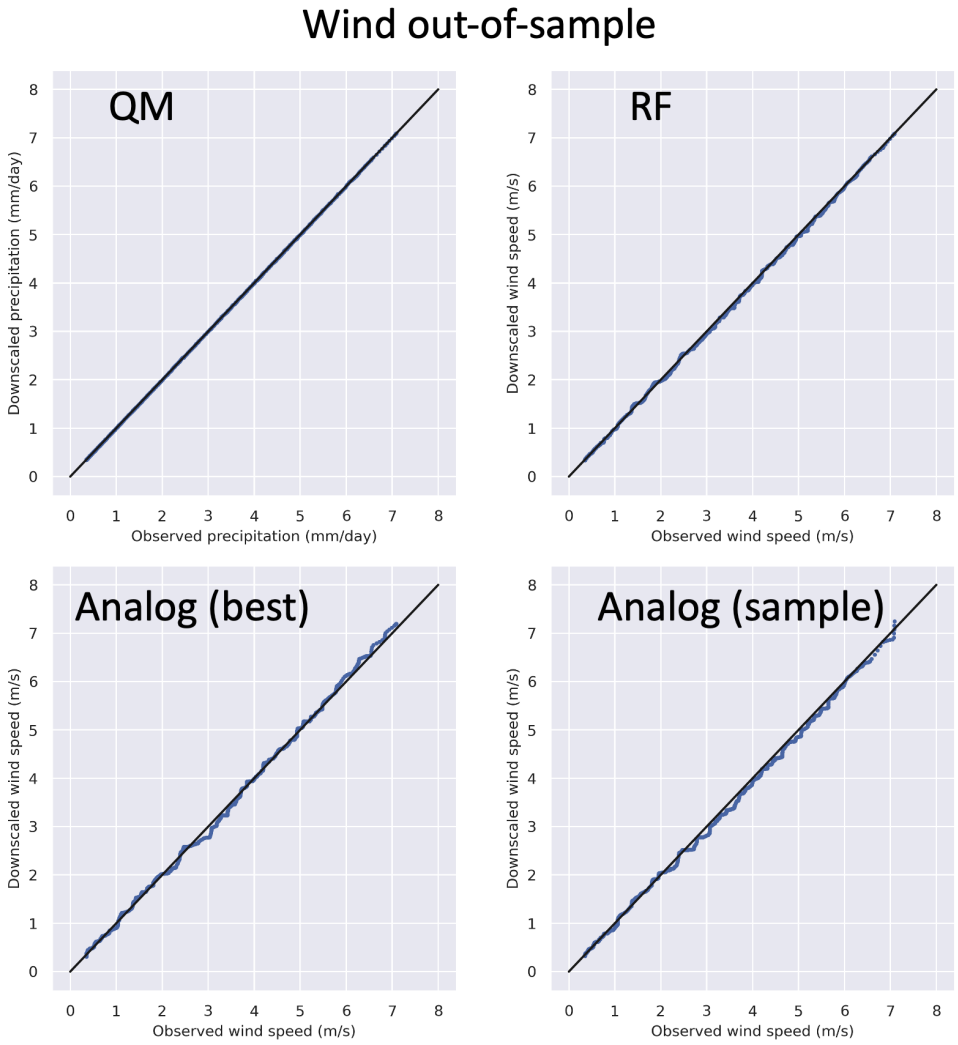

Figure 5: As in Figure 3, but for daily average **wind speed**.

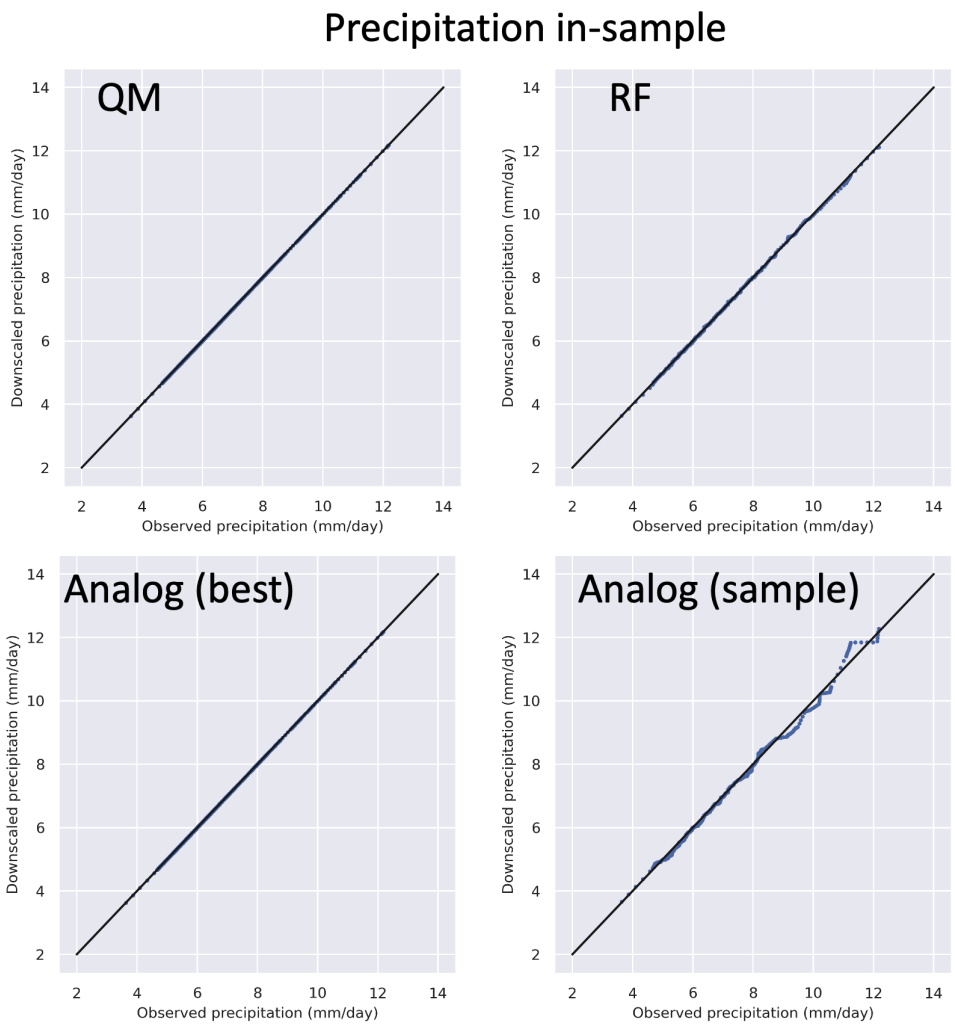

Figure 6: As in Figure 2, but for cumulative daily **precipitation**.

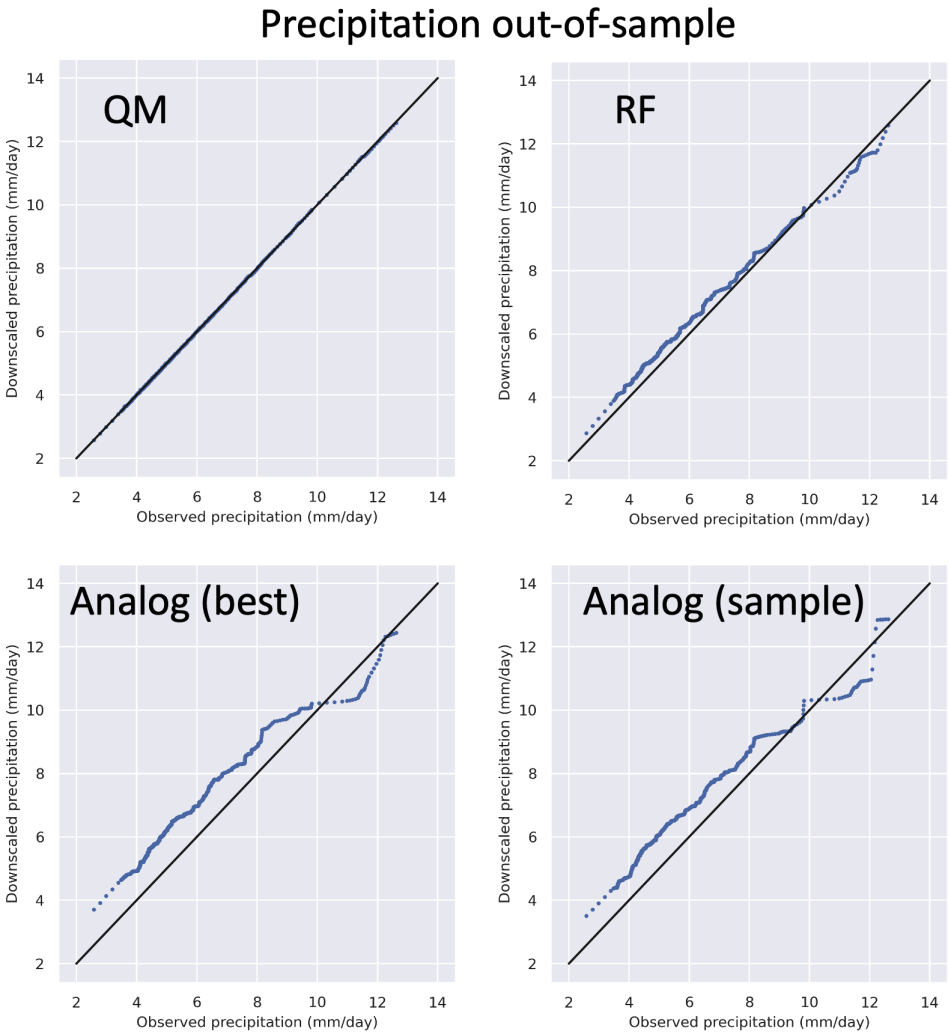

Figure 7: As in Figure 3, but for cumulative daily **precipitation**.

4 Coastal surge model

There is evidence that the frequency of tropical cyclones has been increasing in coastal regions during the last decades, with higher central wind intensity compared to the past (e.g., Wang and Toumi, 2021, 2022a,b). Due to the coarse resolution of CMIP-6 models, some coastal weather systems with high wind, such as typhoons, cannot be properly simulated. Indeed, the statistically downscaled wind field cannot resolve clearly the wind structure of those weather events even when the downscaled grid spacing is increased to be less than 1 km. Nevertheless, the CMIP-6 model can still generate some coastal wind response in different climate scenarios.

To estimate the surge change due to wind speed response to different future climate pathways, we implement a simple scaling approach relating surge change to current climate state by using as a benchmark a category-2 typhoon making landfall. A category-2 typhoon is chosen here mainly because its intensity level is close to the upper bound of the definition of Minor Tropical Cyclones and its landfall frequency is still quite high. The widely used Saffir-Simpson Hurricane Wind Scale (SSHS) suggests that the surge height may change linearly from 1.5 m to 5.5 m when the coastal wind speed increases from 42 to 69 m/s (i.e., the equivalent maximum wind speed when transitioning from a category-2 to a category-5 typhoon) (see Taylor et al., 2010). The linear sensitivity of surge to wind can therefore be written as 0.15 m / m/s, where $0.15 = (5.5 - 1.5)/(69 - 42)$. In our analysis, we first calculate the relative change of wind for a coastal region, denoted by (say) x%. Second, we assume the extreme wind for this location to increase from 42 m/s by 42 m/s $\times$ x% in the future. Finally, we estimate the surge change for a wind speed increase of 42 m/s $\times$ x% by using the approximate linear relationship between wind speed and surge from the SSHS scale of 0.15 m / m/s. This can be written as 6.3 $\times$ x% m, where $6.3{=}42{\times}0.15$, meaning that the surge change (SC) relative to the current climate can be written as:

$$SC = 6.3\frac{W_f}{W_c}, \tag{1}$$

where W_f and W_c denote the surface wind speed at a given location in the future and current climate, respectively. Equation (1) shows that with the current scaling method the estimated surge change is fully driven by the relative change in surface wind speed. This is clearly a simplification, as storm surge is shaped by other factors, such as wind speed direction relative to the coastline and cyclone moving speed at landfall. However, we believe the simplification offers a good compromise, given the inability of CMIP models to properly resolve tropical cyclones and the difficulty to include other factors within a direct statistical downscaling approach. It should be noted that the surge downscaling reported here is on top of the sea level rise, i.e., the excess water level change. Sea level rise projections based on the IPCC AR6 report can be accessed via the NASA sea level projection portal. An increase of between 0.23 and 0.24 meters is projected for the locations of interest in this study under RCP8.5-2050.

5 Typhoon risk assessment

The CMIP6 model can simulate some cyclonic systems directly in the Southeast Asian region. With the statistical downscaling method used in our report, the future changes in precipitation and wind speed are related to the cyclonic weather systems in an indirect manner. Due to the limitation of coarse resolution of the CMIP6 models, the temporal-spatial scale of actual cyclones can be very different. This makes it hard to directly generate reliable heavy precipitation, high wind, and therefore storm surge induced by severe storms such as typhoons. This is the reason why we use the relative change in wind speed to project coastal surge changes along the chosen climate scenario.

In future work, researchers from Imperial College London will start utilizing a new downscaling tool, i.e., the Imperial College stochastic weather generator, to enhance the CMIP6 model simulations so that we may have more accurate estimates of low probability weather events with high economic impacts. The analysis will go beyond typhoon risk and include the following hazards:

1. typhoon (with priority),
2. excess precipitation (flood),
3. drought, and
4. fire risk index.

The four hazards will be examined in terms of their recent relationship with El Nino. Long range projections will be produced by using the ocean's subsurface temperature. Publicly available monthly to multi-season numerical model projections in the CMIP6 models will be examined as multi-model ensembles in combination with the stochastic model to develop risk indices for these four hazards on time scales ranging from weeks to multiple years. Work on hazards 1-4 will contribute to research activities on nature-based solutions as part of both the Climate Risk Scenario and Nature Based Solutions workstreams.

References

Cressie, N. (1993). *Statistics for Spatial Data*. John Wiley & Sons, New York.

Lorenz, E. N. (1969). Atmospheric predictability as revealed by naturally occurring analogues. *Journal of Atmospheric Sciences*, 26(4):636–646.

Maraun, D. (2013). Bias correction, quantile mapping, and downscaling: Revisiting the inflation issue. *Journal of Climate*, 26(6):2137–2143.

Pang, B., Yue, J., Zhao, G., and Xu, Z. (2017). Statistical downscaling of temperature with the random forest model. *Advances in Meteorology*, 2017.

Panofsky, H. A. and Brier, G. W. (1968). *Some applications of statistics to meteorology*. Earth and Mineral Sciences Continuing Education, College of Earth and â¦.

Taylor, H. T., Ward, B., Willis, M., and Zaleski, W. (2010). The saffir-simpson hurricane wind scale. *Atmospheric Administration: Washington, DC, USA*.

Thrasher, B., Maurer, E. P., McKellar, C., and Duffy, P. B. (2012). Bias correcting climate model simulated daily temperature extremes with quantile mapping. *Hydrology and Earth System Sciences*, 16(9):3309–3314.

Van den Dool, H. (1994). Searching for analogues, how long must we wait? *Tellus A*, 46(3):314–324.

Wang, S. and Toumi, R. (2021). Recent migration of tropical cyclones toward coasts. *Science*, 371(6528):514–517.

Wang, S. and Toumi, R. (2022a). More tropical cyclones are striking coasts with major intensities at landfall. *Scientific reports*, 12(5236):1–8.

Wang, S. and Toumi, R. (2022b). On the intensity decay of tropical cyclones before landfall. *Scientific reports*, 12(1):1–8.